Influence of the dispersion characteristics for producing thermoregulating nano phase change slurries.

D. López-Pedrajas[1], A. M. Borreguero[1], F. J. Ramos[1,2], J. F. Rodríguez[1], M. Jiménez-Vázquez[1], M. Carmona[1*]

[1]*Department of Chemical Engineering, Institute of Chemical and Environmental Technology, University of Castilla-La Mancha, Avda. De Camilo José Cela s/n, 13071 Ciudad Real, Spain.*

[2]*Department of Vegetal Production and Agricultural Technology, Higher Technical School of Agricultural and Forestry Engineering, University of Castilla-La Mancha, Pº de los Estudiantes s/n, 02006 Albacete, Spain*

*Corresponding author: e-mail: Manuel.CFranco@uclm.es

Abstract

Phase Change Dispersions (PCDs) of large colloidal stability were produced by sonication at an energy per liquid volume of ~800 kJ L^{-1}, using gum arabic (GA) and sodium dodecyl sulfate (SDS) mixtures as dispersant agent and varying their mass ratios from 0 to 100 (GA/SDS). An important interplay between the PCD base properties and the final phase change slurry (PCS) characteristics was observed, finding that the PCD with the minimum breaking ratio, promotes the PCS with the largest colloidal stability. PCSs from GA/SDS mass ratios of 70/30 and 40/60 were homogeneous, whereas those ones from mass ratios 20/80 or 0/100 generated two phase products. The PCS prepared with a 40/60 of GA/SDS mass ratio was the unique slurry that satisfied the European classification as nanomaterial with a $dn_{0.5}$ of 94.7 ± 15.0 nm. This homogenous nano-slurry (NPCS) had a solid concentration of 28.1 wt% and large latent heat (32.8 J g^{-1}), exhibiting thermal reversibility, long-term colloidal stability ($|\zeta|$ =53.4 ± 1.8 mV freshly

and $|\zeta| = 55.86.3 \pm 6.3$ mV after two years) and Newtonian behavior with low viscosity (10.7 ± 0.3 mPa·s). Besides, observing the encapsulation efficiency, the best reaction was performed producing this nano-slurry with a particle yield of 72.3 % and a PCM content in the capsules close to 50%.

Keywords: Phase change material, cosurfactants, nanoencapsulated PCM slurry, thermal fluid, thermal energy storage

Abbreviations

BPO	Benzoyl peroxide
C_{PCM}	PCM content in the capsules
DLS	Dynamic light scattering
$dn_{0.5}$	Particle size in number
DSC	Differential scanning calorimetry
$dv_{0.5}$	Particle size in volume
DVB	Divinylbenzene
EE	Encapsulation efficiency
GA	Gum Arabic
HRSEM	High resolution scanning electron microscopy
MPCS	Microencapsulated PCM slurry
NPCM	Nanoencapsulated PCM
NPCS	Nanoencapsulated PCM slurry
PCD	Phase change dispersion
PCM	Phase change material
PCS	Phase change slurry
PV	Photovoltaic solar collectors
PV/T	Photovoltaic thermal hybrid solar collectors
RT27	Paraffin rubitherm$^@$RT27
S	Styrene
SDS	Sodium dodecyl sulfate
S~DVB@RT27	Capsules synthesized in this research after washing, without non encapsulated paraffin
S~DVB@RT27/RT27	Solids phase of the PCSs after water evaporation, it is form by the capsules and non-encapsulated PCM

SPCM	Submicroencapsulated PCM
SPCS	Submicroencapsulated PCM slurry
s-S~DVB@RT27	Slurries synthesized in this research
TES	Thermal energy storage
TGA	Thermogravimetric analysis
$W_{Monomers}$	Amount of the monomers fed
W_{PCM}	Amount of pure PCM fed
$W_{S\sim DVB@RT27/RT27}$	Weight solid contents after water evaporation
$W_{S\sim DVB@RT27}$	Weight solid contents after water evaporation and washing stage
ΔH_{PCM}	Latent heat of pure PCM (RT27)
$\Delta H_{S\sim DVB@RT27/RT27}$	Latent heat of dried capsules without the washing step
$\Delta H_{s\text{-}S\sim DVB@RT27}$	Latent heat of dried capsules after the washing step
$\eta_{S\sim DVB@RT27}$	Particle yield
Z	Zeta potential
$|\zeta|$	Zeta potential in absolute value

1. Introduction

One of the current major challenges for society is satisfying the high and rising energy demand with sustainable and environmentally friendly energy sources. Solar energy is considered one of the most promising renewable energy alternatives combining zero cost, abundance and lack of emissions [1]. The utilization of this kind of energy can reduce the dependence on the fossil fuels. However, due to its intermittency, special arrangements have to be made for its adaptability [2]. For instance, the use of thermal energy storage (TES) in buildings can mitigate the problem of temperature fluctuations [3]. There are three main approaches for TES: sensible heat storage, latent heat storage and thermochemical energy storage [4]. Latent heat storage refers to heat transfer associated with phase transitions. The main advantage of latent heat storage is the high energy storage density in narrow temperature ranges. The materials used for latent heat storage are known as phase change materials (PCMs). These materials are able to absorb,

store and release energy during the phase change. In fact, PCMs have been implemented in passive energy storage systems since 1980 [5] by their incorporation in walls, shutters, ceilings and floors, using building materials such as gypsums, concrete and polyurethane foams [6–12]. However, the employment of PCMs presents some limitations, being necessary to avoid leakage during solid-liquid transitions. To prevent this leakage, the PCM must be adequately contained, for example by its encapsulation inside a shell of polymeric material [13–17].

Furthermore, PCM capsules can be incorporated in a fluid, forming Phase Change Slurries (PCSs), permitting their transport, pumping and implementation in active energy storage systems [18]. The active energy storage strategies cover heating, ventilation, and air conditioning systems, where PCSs can be widely applied. Moreover, photovoltaic thermal hybrid solar collectors (PV/T) can use this kind of dispersions as thermal fluids, reducing the working temperature of the PV panel. This way, PV/T systems with thermoregulating slurries produce electricity more efficiently than conventional PV ones; at the time that the solar thermal part of the PV/T provides heat [19,20].

Regarding the size of the capsules dispersed in the PCS, microencapsulated PCM slurries (MPCSs) have been widely studied for heating and cooling purposes due to their high heat transfer capacity as heat transfer fluid [18,21–23]. However, flocculation and settling of the solid particles after the slurry production are not easily controllable since the particles often aggregate. The undesirable aggregation and settling effects reduce the stability of the slurry and worsen the fluid properties [24,25]. In the recent years, the research efforts have been focused on the manufacture of submicron- (SPCSs) or nanoencapsulated PCM slurries (NPCSs), since they presented better long-term stability, higher heat transfer area and better structural stability by reducing the capsule size [4,26–

28]. Thus, one of the key parameters which determines the final properties of PCSs is the size of the dispersed solid particles.

One of the early steps for NPCS manufacturing is the dispersion of the PCM material in the liquid medium, usually aqueous, in order to prepare the phase change dispersions (PCDs). PCDs can be classified according the droplet size, the stability lifetime and the typical particle size of the capsules prepared from such dispersion into emulsions (1-10 μm of droplet size, stability from seconds to months and > 1 μm of particle size), miniemulsions (20-200 nm of droplet size, stability from hours to months and 100-300 nm of particle size) and microemulsions (10-100 nm of droplet size, infinite stability and 30-100 nm of particle size) [29]. Among them, miniemulsions are excellent precursors for the formation of submicron capsules (SPCMs) and nanocapsules (NPCMs) containing PCM [4]. They can be achieved using common homogenization systems, such as high-power stirrers (Ultraturrax) or ultrasonication devices. Stirrers meet certain issues as their limited power and losses by friction [30], whereas sonicators can be employed for a wide variety of applications in the field of materials chemistry, since they are very effective in reducing the droplet size of dispersed oily phases [31].

However, more important than the homogenization system is the type and concentration of the dispersing agent chosen for the preparation of stable PCDs with acceptable particle size. Different dispersants have been used to fabricate PCSs with submicronic and nanometric capsules size, such as, sodium dodecyl sulfate (SDS) [32], SDS in combination with polyethylene glycol mono(octylphenyl) ether [33,34], NP-10 [35] and triton X-100 [36]. Table 1 lists the main properties of SPCSs and NPCSs and their capsules that can be found in the literature. On the other hand, some authors highlight the effectiveness of the addition of co-surfactants to improve the stability of the dispersion and reduce the overall amount of dispersant [37,38]. Regarding the fabrication of

thermoregulating submicron-/nanoslurries, up to date, the main manufacturing route consists in the synthesis, separation and purification of the submicron-/nanocapsules and their further re-dispersion in a liquid media different from the reaction one [32–35,39]. The major problems associated to this methodology are the excessive consumption of materials, the large waste generation, the low solid concentration, and so, the poor heat capacity of the final thermoregulating fluid. In contrast, in this study, the NPCS is produced directly *in situ* from a stable PCD. Then, the polymerization reaction takes place in the PCD media to form the shell material around the PCM droplets; leading to a single product without further separation, cleaning or additional purification procedures. In that way, the quantification of non-encapsuled paraffin present in the slurry is also needed.

The introduction of cosurfactant mixtures has been an approach poorly exploited for obtaining NPCSs. In this research, the employment of mixtures of gum arabic (GA) and sodium dodecyl sulfate (SDS), two of the most extensively known and utilized dispersants, has been investigated [32–34,40]. The influence of the sonication energy per dispersion volume on the paraffin droplet size and the effect of the GA/SDS mass ratio on the PCD breaking ratio has not been reported yet in literature. In this way, the cosurfactant mass ratio was assessed not only for the prepared PCDs, but also for the final PCS.

The NPCSs reported in literature are frequently catalogued as nano- even without satisfying the ISO criteria [32–35,39]. However, in this research, it is achieved a homogeneous and stable NPCs by the optimization of the cosurfactants ratio. The slurries are going to be synthesized using *in situ* polymerization technique, taking advantage of the experience of our group in heterogeneous phase polymerization [41–45]. For preparing the homogenous PCSs with a solids content up to 28.1 wt%, the GA/SDS mass ratio is going to be varied from 100/0 to 0/100, analysing the particle size distribution for

6

doing the classification as nano or sub-micron slurry. The dispersant mixture mass ratio (GA and SDS) was changed with the aim to achieve the optimal value that led more stable PCD, allowing to manufacture a homogeneous NPCS with large solid content, low particle size, colloidal stability, low viscosity and remarkable thermal properties.

2. Experimental section

2.1. Materials

Table 2 lists the materials used for the research development. All materials were used as received, except for the S and DVB monomers. They were subjected to a purification process to remove the polymerization inhibitor by using three successive washes with a solution of NaOH in water (1.25 N) and a further rinsing with water. NaOH washing solution was prepared homemade from pellets.

2.2. Preparation of Phase Change Dispersions (PCDs)

For the preparation of the PCDs, the PCM content was fixed at 17.8 wt% and it was stabilized in water using a mixture of dispersants (GA/SDS), changing its mass ratio from 100/0 to 0/100, being the dispersant amount a 20 wt% of the added PCM [46]. The detailed process for the preparation of o/w PCDs is detailed in our patent application [47]. In brief, the required amount of cosurfactant was dissolved in water by agitation. After that, the molten PCM was added, and the paraffin/water system is subjected to ultrasonication for the time needed to reach the desired PCD droplet size.

2.3. Synthesis of thermoregulating slurries (PCSs)

The PCSs were synthesized by *in situ* polymerization technique according to the previously reported procedure [47]. In detail, the reactor consists of a 0.25 L jacketed glass vessel, equipped with a Rushton turbine stirrer with six vertical blades, a reflux

condenser and a digital stirring control, nitrogen gas connection and a thermostatic bath to keep the reaction at the desired conditions. Inside such reactor, PCM/water PCDs were prepared using GA/SDS mass ratios of 100/0, 70/30, 40/60, 20/80 and 0/100 for the slurry fabrication. In a separated vessel, a prepolymerization reaction between co-monomers (S and DVB, in equal mass quantities) was started at 50 ºC in the presence of BPO as initiator and under stirring. After 25-30 minutes of prepolymerization, this mixture was dropwise poured over the corresponding PCD, keeping the reaction mixture under stirring and heating (70-80 ºC) for 5 h. In Table 3 it is shown the amount (wt%) of the reagents used for the PCSs production.

After reaction, the product was cooled down and stored without any further purification or post-treatment and they were named as s-S~DVB@RT27$_x$, being x the corresponding GA/SDS mass ratio. For products constituted by two separated phases, presenting both good stability and fluidity, a "*" symbol was included to indicate the upper separated phase.

A scheme of PCD and PCS production is shown in Fig. 1.

2.4. Characterization

2.4.1. Zeta potential (ζ) measurements.

Colloidal stability of the synthesized fluids was analyzed by zeta-potential (ζ) measurements with a Malvern Instruments Z-Sizer Nano ZS. The equipment employs a Doppler laser microelectrophoresis technique, being able to determine the ζ of a suspension with particle diameters comprised between 3.8 nm and 100 μm according Smoluchowski's equation.

2.4.2. PCD breaking ratio.

The breaking ratio was used to measure the degree of instability of the prepared PCDs (both fresh and after 15 days), which break into a watery bottom phase and an oily upper one. PCDs were poured inside a plastic graduated cylinder at 50 °C for 15 days. Thus, the PCM that could not be emulsified appears as an upper separated phase. The breaking ratio was calculated following the next Equation [1]:

$$Breaking\ ratio\ (\%) = \frac{Separated\ PCM\ Volume\ \cdot \rho_{PCM}}{W_{PCM}} \times 100\ [1]$$

where W_{PCM} is the total amount of pure PCM fed, and ρ_{PCM} its density.

2.4.3. Gravimetry.

The solid content, expressed as weight percentage (wt%), was calculated by gravimetry. Slurry samples were dried for 8 hours at 50 °C, to ensure the complete water evaporation. The obtained solids considering the impregnated or non-encapsulated paraffin were named as S~DVB@RT27/RT27$_x$ and they were further washed with an ethanol and water mixture (50/50 vol%) and called as S~DVB@RT27$_x$; being x, in both cases, the corresponding GA/SDS mass ratio. In this way, two solid contents were determined, $W_{S~DVB@RT27/RT27}$ and $W_{S~DVB@RT27}$, corresponding with the weight change from the initial slurry to the final solids, after water evaporation or water removal and washing stage, respectively.

2.4.4. Dynamic Light Scattering (DLS).

Particle size distribution in volume (*dv*) and number (*dn*) of S~DVB@RT27 from the synthesized s-S~DVB@RT27, together with its median particle size *dv$_{0.5}$* and *dn$_{0.5}$*, respectively, were determined by Dynamic Light Scattering (DLS), using a Malvern

Instruments Z-Sizer Nano ZS. Polydispersity index (PDI) was calculated according to ISO standard 22412:2017 [48].

2.4.5. Surface tension.

The surface tension of water with dispersants and the PCDs were determined using a Theta optical tensiometer (Attension, Espoo, Finland). Measurements were performed using the pendant drop method at room temperature.

2.4.6. High Resolution Scanning Electron Microscopy (HRSEM).

SEM studies were performed using a HRSEM model GeminiSEM 500 (ZEISS) working at 2 kV. Samples for SEM observation were prepared by depositing droplets of diluted s-S~DVB@RT27 of the samples onto a holey carbon grid (EMS) and waiting at room temperature until the evaporation of water.

2.4.8. Thermogravimetric analysis (TGA).

Thermogravimetry analysis (TGA) of both, s-S~DVB@RT27 and S~DVB@RT27, were carried out with a SDT Q600 Simultaneous DSC-TGA from TA Instruments, using a heating rate of 10 ºC·min^{-1} from room temperature to 700 ºC, under nitrogen atmosphere.

2.4.9. Differential scanning calorimetry (DSC).

Latent heat storage capacities and melting point were determined by a differential scanning calorimetry model DSC Q100 of TA Instruments equipped with a refrigerated cooling system and nitrogen as the purge gas. The test temperature ranged from – 40 to 45 ºC with a heating and cooling rate of 3 ºC·min^{-1}, according to our previous results, although in literature is recommended to carry out this analysis at a heating rate as slow as possible (0.5 K/min) [49]. Before these heating and cooling ramps, the thermal history

of the material is eliminated by cooling, from room temperature to - 40 ºC with a cooling ramp of 10 ºC min^{-1}, and with an isothermal of 1 min. Both, liquid and solid samples, were analyzed with the same procedure. Latent heats in J g^{-1} of pure RT27 (ΔH_{PCM}), of dried solid capsules contained in the slurry before ($\Delta H_{S\sim DVB@RT27/RT27}$) and after washing ($\Delta H_{S\sim DVB@RT27}$), together with the latent heat storage capacity of the PCS ($\Delta H_{s\text{-}S\sim DVB@RT27}$) were obtained through this method. The washing process was carried out in order to accomplish a right quantification of the encapsulated paraffin, removing the impregnated RT27 paraffin from the S~DVB@RT27 by using a mixture water/ethanol 50/50 by weight after the slurry water evaporation. Finally, the capsules were left overnight on an absorbent paper at 50 ºC, for their drying. A thermal heating /cooling cycle was performed between high and low temperatures of 40 ºC and –10 ºC, respectively, at a ramp rate of 3.0 °C min^{-1}. This temperature interval was carefully chosen to be representative of the PCS potential working condition. All DSC tests were carried out twice and the reported values correspond with the average data.

2.4.10. Shear Rheometry.

Rheological properties of s-S~DVB@RT27 were measured by rotational viscometry using a Malvern Instruments BOHLIN GEMINI^{TM} 200. The CP50 cone&plate system with water trap was used to test the synthesized products. The cone has 50 mm of diameter and 1º of angle. The plate is equipped with a Peltier cell for temperature control. Measurements were repeated three times with fresh samples, ensuring the reproducibility of the results. The temperature was controlled at 20 ºC and the shear rate was varied according to the cycle of 1 - 250 - 1 s^{-1}.

Surface tension, ζ, viscosity, $dv_{0.5}$ and $dn_{0.5}$ were measured four times to obtain the confidence interval (mean ± error), using $\alpha = 0.05$.

2.5 Determination of PCM content (C_{PCM}), encapsulation efficiency (EE) and particle yield ($\eta_{S\sim DVB@RT27}$)

The PCM content (C_{PCM}) of the capsules was calculated based on the latent heats of capsules (after non-encapsulated PCM removal) and the pure PCM:

$$C_{PCM} \, (\%) = \frac{\Delta H_{S\sim DVB@RT27}}{\Delta H_{PCM}} \times 100 \quad [2]$$

where $\Delta H_{S\sim DVB@RT27}$ and ΔH_{PCM} are the latent heats (J g^{-1}) of the dried capsules (S$\sim$DVB@RT27$_x$) and the pure PCM, respectively.

The encapsulation efficiency (*EE*) can be obtained from the relationship between the encapsulated PCM and the total mass of PCM fed:

$$EE \, (\%) = \frac{W_{S\sim DVB@RT27} \cdot \Delta H_{S\sim DVB@RT27}}{W_{PCM} \cdot \Delta H_{PCM}} \times 100 = C_{PCM} \times \frac{W_{S\sim DVB@RT27}}{W_{PCM}} \quad [3]$$

where $W_{S\sim DVB@RT27}$ and W_{PCM} are the weights of the dried capsules and the pure PCM fed in the reactor, respectively.

The capsule yield ($\eta_{S\sim DVB@RT27}$) is expressed as the mass of capsules in the final product divided by the mass of reagents fed to synthetize those capsules (Eq. 4):

$$\eta_{S\sim DVB@RT27}(\%) = \frac{W_{S\sim DVB@RT27}}{W_{PCM} + W_{Monomers}} \times 100 \quad [4]$$

where the $W_{Monomers}$ is the mass of monomers fed to the reactor.

Unfortunately, the separation of S$\sim$DVB@RT27 from the s-S$\sim$DVB@RT27 by filtration techniques resulted unfeasible in this case, since a great part of the capsules can cross the filter barrier together with the liquid media due to the nanometric capsule size. Then, the total amount of capsules is not easy to be assessed. Moreover, the amount of PCM enclosed in the capsule cannot be easily distinguished from the PCM that remains

out of the capsule, normally emulsified, making necessary the washing step previously detailed in Characterization section. However, after such washing step for removing the non-encapsulated paraffin, the washed capsules (S~DVB@RT27) cannot be fully separated again by filtration. So, it is not possible to determine $W_{\text{S~DVB@RT27}}$ by direct weight measurements (neither gravimetry nor TGA). Consequently, in order to obtain the real mass of capsules ($W_{\text{S~DVB@RT27}}$), and then, EE and $\eta_{\text{S~DVB@RT27}}$, mass and energy balances were needed, according:

$$W_{\text{S~DVB@RT27}} = \frac{\Delta H_{\text{S~DVB@RT27/RT27}} - \Delta H_{PCM}}{\Delta H_{\text{S~DVB@RT27}} - \Delta_{PCM}} \times W_{\text{S~DVB@RT27/RT27}} \quad [5]$$

3. Results and discussion

3.1. Effect of GA/SDS ratio on PCD stability and droplet size

PCD stability was evaluated analyzing the breaking ratio of the PCDs, the droplet size of the PCM micelles (PCD droplet size) and their ζ, which are parameters commonly used for this purpose [24,50,51].

Firstly, the effect of sonication time (also expressed as sonication energy given to the PCDs divided by their volume) upon PCD droplet size ($dn_{0.5}$ and $dv_{0.5}$) and its corresponding $|\zeta|$ is shown in Fig. 2.In Fig. 2, it can be observed that the $dv_{0.5}$ and $dn_{0.5}$ decrease with the sonication time, since the total sonication energy applied for a PCD volume provokes a breaking of the paraffin droplets as the sonication is lengthened. However, the droplet size was stabilized for an energy/volume of ~800 kJ L^{-1} (reached at ~ 9 min of sonication). It was also distinguished that PCD kept good stability at this time, according to the $|\zeta|$ (> 30 mV) [52,53]. So, the experimental sonication time of all PCDs was adjusted accordingly.

The breaking ratio of the synthesized PCDs is shown in Fig. 3a, together with a photograph after 15 days of settling for the PCDs with the highest and lowest breaking ratios (Fig. 3b).

As illustrated in Fig. 3a, the minimum breaking ratios, with values around 2 vol%, can be found for GA/SDS mass ratios ranging between 50/50 to 30/70 for fresh PCDs. In contrast, the PCD from a GA/SDS mass ratio of 100/0 presented the highest breaking ratio, attaining up to 19.0 vol%, just after preparation. After 15 days, the o/w PCDs exhibited the same general trend than fresh ones. However, the absolute values of breaking ratios increased for all the surfactant mixtures, growing more for those ones that were more unstable freshly prepared. Attending to Fig. 3a, the optimal GA/SDS mass ratio is easily identified, since the breaking ratio of the mixture 40/60 was the one which remained lower after 15 days of settling (only 2.1 vol%). In Fig. 3b, it can be appreciated the appearance of the PCD from the optimal GA/SDS mass ratio (40/60) after 15 days of settling, showing two different phases: a very thin upper one, formed by separated paraffin, and the desired PCD at bottom. The rest of GA/SDS mass ratios showed the same two phases except the 100/0, which split in three different phases after 15 days of settling (Fig. 3b): an upper phase constituted of pure paraffin (~13.0 vol%, red bar); a low concentrated dispersion at the bottom part mainly made up of water (~70.6 vol%, yellow bar) and an intermediate phase (~ 16.4 vol%, blue bar), consisting in a concentrated paraffin dispersion in water.

Fig. 4 shows the PCD droplet size and the |ζ|, measured by DLS and Doppler laser microelectrophoresis techniques, respectively, for the fresh PCDs and after 15 days of settling.

According to the |ζ| (Fig. 4a), it was possible to obtain stable PCDs independently the GA/SDS mass ratio employed, since all of the |ζ| values were higher than 30 mV, the

extendedly accepted criteria to consider a PCD as stable [52,53]. This is true even for the PCD from a GA/SDS mass ratio of 100/0. Besides, PCDs from intermediate mixtures of surfactants revealed a maximum in PCD stability, since larger values of the $|\zeta|$ were obtained, agreeing with the optimal dose (GA/SDS = 40/60) according to the breaking ratio results. After 15 days of preparation, $|\zeta|$ decreases for all the surfactant mixtures, but the stability standards of PCDs ($|\zeta| > 30$ mV) were kept [52,53]. In the case of using only with GA as surfactant, the PCD exhibited a reasonable value of $|\zeta| = 42.7 \pm 1.2$ mV freshly but it was separated after 15 days of settling in two poorly stable PCDs, with 32.3 ± 1.7 and 37.0 ± 0.6 mV for the upper and bottom (clarified) phases, respectively.

Regarding the droplet size (Fig. 4b), the increase of SDS content up to a 40 wt% in the surfactant mixture caused a sharp decrease in the $dn_{0.5}$ and $dv_{0.5}$ of the emulsified paraffin droplets, reaching a plateau for mixtures with SDS contents ≥ 50 wt%. The $dn_{0.5}$ and $dv_{0.5}$ were quite similar, revealing the low dispersibility of the PCDs, attending to the droplet size distributions. In detail, for fresh PCDs, the droplet diameter presented $dv_{0.5} = 83.7 \pm 18.4$ and $dn_{0.5} = 61.5 \pm 8.6$ nm for the smallest droplets made from GA/SDS mass ratio of 20/80. Using only GA, it was not possible to obtain neither small droplets nor a narrow size distribution, since this product had droplet diameter range from 225 nm up to 6 μm. The reason for the droplet size differences in PCDs when using pure GA, pure SDS or their mixtures, can be related with the smaller critical micelle concentration (CMC) of SDS (2.3 g L^{-1}) [54] respect to that of GA (126.5 g L^{-1}) [55], being higher the capability of SDS to form stable dispersions. After 15 days, the trend for most of the PCDs was the same, only observing a moderate increase in the droplet size (both for $dv_{0.5}$ and $dn_{0.5}$), related to collision and coalescent phenomena due to Brownian movement. Attending to the Rao, J. P. *et al.* classification [29], PCDs from mass ratios of 40/60 to 0/100 could be classified as miniemulsion, because they presented a median particle size

between 20 - 200 nm, good stability and low polydispersity. According European Commission and ISO criteria [56,57], fresh PCDs from GA/SDS mass rations of 70/30 to 0/100 can be also classified as nanomaterials, because more than 50 % of the components in the final product (emulsified droplets in this case) showed a diameter comprised within 1 - 100 nm.

Considering all the studied techniques, the GA/SDS mass ratio 40/60 has been found as the ideal relationship for preparing PCDs, since $PCD_{40/60}$ presented the lowest breaking ratio after 15 days, together with nanometric droplet size and remaining in the interval of better colloidal stability according to ζ values. In order to explain this behavior, the surface tension of the studied PCDs was measured (Fig. 5).

From these results, it can be concluded that having a low surface tension in the mixture water-cosurfactant is essential for the good stability of the PCD. A low surface tension promotes that the whole system behaves as a unique phase, avoiding or hampering the phase separation. This also explains the phase separation observed in the case of a GA/SDS mass ratio of 100/0. Moreover, in the view of previous works, this reduction in the surface tension is linked to the final morphological properties of the PCM capsules, showing a core-shell structure and higher encapsulation efficiency when the surface tension and the polarity of the surface were reduced [42,58].

Then, for PCS manufacturing, different GA/SDS mass ratios will be tested. In particular, the GA/SDS examined were the ones that promoted different PCD characteristics (100/0, 70/30, 40/60, 20/80 and 0/100), to assess the influence of the PCD characteristics on the final NPCS properties.

3.2. Effects of GA/SDS mass ratio on PCS

The feasibility to produce thermoregulating aqueous stable slurries constituted by capsules with styrene-divinylbenzene copolymer (S/DVB mass ratio = 50/50) as shell and containing Rubitherm®RT27 as PCM by using GA/SDS mass ratios of 100/0, 70/30, 40/60, 20/80 and 0/100 was analyzed by observing the breaking ratio of such products (Fig. 6).Fig. 6a shows that just those products from GA/SDS mass ratios of 70/30 and 40/60 were homogeneous fluid products presenting only one phase, which is in good agreement with the results obtained from breaking ratios, $|\zeta|$, droplet sizes and surface tension of the PCDs prepared before polymerization reaction. In contrast, three separated phases appeared in the product from 100/0 of GA/SDS mass ratio. Due to its instability and lack of fluidity, this product was not further characterized. On the other hand, in the case of the products from GA/SDS mass ratios of 20/80 and 0/100, another fluid product appeared after 2 days, splitting finally into two well-distinguished fluid phases, corresponding to two different homogeneous slurry products with upper phases having relative volumes of 30 and 45 vol%, respectively.

Thus, six different slurries can be perfectly distinguished, s-S~DVB@RT27$_{30/70}$, s-S~DVB@RT27$_{40/60}$, s-S~DVB@RT27$_{20/80*}$, s-S~DVB@RT27$_{20/80}$, s-S~DVB@RT27$_{0/100*}$ and s-S~DVB@RT27$_{0/100}$, where "*" means the upper separated slurry.

In order to know the particle size distribution (PSD) of the different PCSs, DLS measurements were carried out (Fig. 7). As can be seen, slurries s-S~DVB@RT27$_{40/60}$, s-S~DVB@RT27$_{20/80}$ and s-S~DVB@RT27$_{0/100}$ satisfy the criterion to be considered as a nanomaterial according ISO standards [56,57], exhibiting $dn_{0.5}$ of 94.7 ± 15.0, 92.8 ± 15.8 and 95.0 ± 9.1 nm and so, these slurries can be named as nanoencapsulated PCM slurries (NPCSs). On the other hand,

three sub-micron slurries were obtained, the s-S~DVB@RT27$_{70/30}$ and the upper

phases s-S~DVB@RT27$_{20/80*}$ and s-S~DVB@RT27$_{0/100*}$, with $dn_{0.5}$ of 150.3 ±

39.3, 120.2 ± 24.2 and 127.5 ± 16.3 nm, respectively. Independently of the

classification of the slurries attending to their $dn_{0.5}$, all of them present monomodal

particle size distribution, being the particle size distribution narrow for NPCSs

and wider for the sub-micron ones. Considering polydispersity, the PDI of NPCSs

were within 0.125 - 0.136 whereas those from sub-micron slurries were between

0.175 and 0.191, where the higher limits represent the homogeneous slurries (s-

S~DVB@RT27$_{40/60}$ and s-S~DVB@RT27$_{70/30}$, respectively). These values

indicate that NPCSs were also more monodisperse products than those classified

as sub-micron slurries. Hence, the breaking ratio that takes place in the slurries

from PCD$_{20/80}$ and PCD$_{0/100}$ could be related with differences in density of the

capsules that constitute the phases, because those particles having the larger size

were located in the upper phase. The difference in density for the capsules forming

the upper or bottom phases can be explained by their PCM content since paraffin

has a lower density (880 kg m^{-3}) than the corresponding polymer shell (~ 1200 kg

m^{-3}).

The relationship between the droplet size from PCDs and the particle size of the

slurries can be observed in Fig. 8.

It is observed that both $dv_{0.5}$ and $dn_{0.5}$ of slurries were undoubtedly higher than

those of the precursor dispersions (PCDs). It means that no new nuclei were formed by

only polymer, but the particle size can be increased by coalescence of paraffin droplets

(Ostwald ripening) and further polymer covering or simply by polymer covering. s-

S~DVB@RT27$_{40/60}$ presented the closest $dn_{0.5}$ and $dv_{0.5}$ to the droplet diameters of the

PCD$_{40/60}$, being just 7.2 and 33.3 nm bigger than their droplets counterparts, respectively.

These results agree perfectly with the minimum breaking ratio obtained for the PCD from a GA/SDS mass ratio 40/60, indicating that this dispersant relationship seems to be the best one for producing homogeneous and monodisperse slurries, since this product is mainly formed by single particles whereas the other slurries are constituted by agglomerated particles or larger particles with more PCM content which tend to separate into an upper phase by flotation. Finally, observing Fig. 8, it is possible to establish the GA/SDS mass ratio intervals for obtaining single products (70/30 - 40/60) or a product split into two different phases (20/80 - 0/100).

Summarizing, the GA/SDS mass ratio of 40/60 was the optimum in terms of breaking ratio and particle size, leading to a NPCS (s-S~DVB@RT27$_{40/60}$) presenting only one homogeneous phase with small diameter and the narrowest particle size distribution.

The morphology of the particles dispersed in the slurry can be appreciated in the HRSEM images collected in Fig. 9.

It can be seen that these nanocapsules present spherical, smooth an independent morphology, not sharing walls between each other. Regarding the size of the capsules, these photos also confirm that the slurries from GA/SDS = 40/60, and the bottom PCS products from 20/80 and 0/100 can be classified as nanomaterials. In contrast, the PCSs from GA/SDS = 70/30 and the upper products from 20/80 and 0/100 show a submicron size. In summary, the capsule size observed by SEM agrees with the one measured with DLS for all the PCSs. On the other hand, for the bigger capsules contained in the separated upper slurries (s-S~DVB@RT27$_{20/80*}$ and s-S~DVB@RT27$_{0/100*}$) a core-shell structure is perceived, which presumably could be present in all of them, although the acceleration employed to take SEM pictures was not sufficient to verify that point in nanometric capsules.

The real solids content of the obtained PCSs was calculated by conventional gravimetry, given 25.3, 28.1, 36.4, 24.7, 32, and 20.1 wt% for s-S~DVB@RT27$_{70/30}$, s-S~DVB@RT27$_{40/60}$, s-S~DVB@RT27$_{20/80*}$, s-S~DVB@RT27$_{20/80}$, s-S~DVB@RT27$_{0/100*}$ and s-S~DVB@RT27$_{0/100}$, respectively.

Another key property for any kind of slurry, independently its application is the viscosity. Shear rheometry measurements were carried out in order to determine the dynamic viscosities at 20 ºC for all PCSs (Fig. 10). It is observed than the s-S~DVB@RT27$_{70/30}$, s-S~DVB@RT27$_{20/80*}$ and s-S~DVB@RT27$_{0/100*}$ exhibited non-Newtonian behavior at low share rates, behaving as pseudoplastic fluids; since the shear stress is not a straight line when plotted as a function of share rate, resulting in higher viscosities at low share rate. The rest of synthesized PCSs exhibited a Newtonian behavior. Considering the dynamic viscosity as the mean variation of shear stress with shear rate in the studied interval, the slurries fabricated had viscosity values of 19.2 ± 2.0, 10.7 ± 0.3, 11.0 ± 2.6, 5.7 ± 0.2, 18.3 ± 3.8 and 3.6 ± 0.5 mPa·s for s-S~DVB@RT27$_{70/30}$, s-S~DVB@RT27$_{40/60}$, s-S~DVB@RT27$_{20/80*}$, s-S~DVB@RT27$_{20/80}$, s-S~DVB@RT27$_{0/100*}$ and s-S~DVB@RT27$_{0/100}$, respectively. Regarding the products that showed phase separation, *i.e.* GA/SDS = 20/80 and 0/100, it is interesting to remark that PCSs from upper phases revealed much higher viscosity than bottom ones, as well as, an non-Newtonian behavior, probably due to significantly higher capsules content. It seems that phase separation promotes the formation of more concentrated slurries in the upper phases. The intermediate mixture of GA and SDS surfactants also show lower viscosity, indicating that the best PCS in terms of fluidity is the s-S~DVB@RT27$_{40/60}$, confirming the conclusions previously pointed out. Furthermore, the rheological behavior of the s-S~DVB@RT27$_{40/60}$ is aligned and even better than those of other slurries with similar concentration. For instance, the PCS obtained for Wu *et al.* with a 28 vol% of NPCMs of

polystyrene as shell and n-octadecane as core reached 2.7 mPa·s at 20 ºC [32]; and Fang and coworkers synthesized a PCS made of *n*-tetradecane nanoencapsulated in poly(styrene-ethyl acrylate) with up to 15 wt% presenting a viscosity of 10 mPa·s at 20 ºC [33].

On the other hand, the stability of these slurries was analyzed once obtained and after two years of preparation. Fig. 11 shows the $|\zeta|$ values for the precursor PCDs, the above mentioned slurries freshly manufactured and after two years of preparation.As can be seen, a good stability of the PCDs ensures the production of slurries having large stability although they lead to two different phases. Nevertheless, it is observed that the worse stable slurry with time is the s-S~DVB@RT27$_{70/30}$ because its $|\zeta|$ value is shifting toward the stability limit of 30 mV. On contrary, the $|\zeta|$ values of the other slurries are moving up to the more stable region, being the s-S~DVB@RT27$_{40/60}$ the product that exhibited the minimum change and also comparable with its precursor PCD$_{40/60}$. Anyway, with the exception of s-S~DVB@RT27$_{70/30}$, it is worthy to remark the great colloidal stability for all these products after two years.

Fig. 12 shows the TGA of the six PCSs synthetized in order to determine their solids content and thermal stability.

Similar weight losses can be observed for all the PCSs. The first one, which had the maximum thermal degradation at 100 ºC corresponds to water evaporation. So, according to TGA the solids content of s-S~DVB@RT27$_{70/30}$, s-S~DVB@RT27$_{40/60}$, s-S~DVB@RT27$_{40/60}$, s-S~DVB@RT27$_{20/80*}$, s-S~DVB@RT27$_{20/80}$, s-S~DVB@RT27$_{0/100*}$ and s-S~DVB@RT27$_{0/100}$ was 26.0, 28.0, 36.9, 23.7, 32.6 and 20.17 wt%, respectively; which are in excellent agreement with the solid content obtained by gravimetry (25.3, 28.1, 36.4, 24.7, 32.0 and 20.1 wt%, respectively). The second weight loss, between 130 and 220 ºC, corresponds to RT27 degradation, including both, the PCM

correctly enclosed inside the capsule and the non-encapsulated paraffin. The paraffin weight loss corresponds to around a 19.0 wt% of the total amount for S~DVB@RT27$_{70/30}$ and s-S~DVB@RT27$_{40/60}$, respectively. It is important to highlight how the upper phases of the PCSs synthesized with GA/SDS mass ratio of 20/80 and 0/100 had a higher amount of PCM with respect to the rest of the PCSs (24.9 and 20.1 %, respectively), due to the lower density of RT27 with respect to water, so if it is not well stabilized it tends to go to the upper phase. On the other hand, s-S~DVB@RT27$_{20/80}$ and s-S~DVB@RT27$_{0/100}$ had the less amount of RT27 (13.5 and 12.8 wt%, respectively) due to the fact that most of it was in the upper phase. According to the TGA decay of the pure SDS, the next weight loss at 220 ºC represents the thermal degradation of its organic part. The fourth weight loss, related to GA degradation, is a slight variation around 310 ºC. The last weight loss is *ca.* 410 ºC and it corresponds with the degradation of the formed S-DVB copolymer.

Then, the latent heat of these slurries and their dried and dried-washed nanocapsules were obtained by DSC. Once knowing the dried solid contents and the above capsule latent heats, the C_{PCM} (Eq. 2), EE (Eq. 3) and $\eta_{S\sim DVB@RT27}$ (Eq. 4) were determined and all results are shown in Fig. 13.DSC curves of the capsules from all the synthesized slurries and pure RT27 are shown in Fig. 13a. As it can be seen, the melting and crystallization temperature ranges of all solid products lay within the corresponding ones of the paraffin, observing even a similar supercooling of about 5 ºC. Nevertheless, it is worthy to remark the light shifting of the melting and crystallization temperatures of S~DVB@RT27$_{20/80*}$ and S~DVB@RT27$_{20/80}$ towards higher temperatures and close to borders of the pure paraffin. In order to explain this behavior, a washing protocol was addressed for allowing to distinguish between the encapsulated paraffin from the non-encapsulated one.

Latent heats ($\Delta H_{S \sim DVB@RT27/RT27}$) of non-washed capsules S~DVB@RT27/RT27$_{70/30}$, S~DVB@RT27/RT27$_{40/60}$, S~DVB@RT27/RT27$_{20/80*}$, S~DVB@RT27/RT27$_{20/80}$, S~DVB@RT27/RT27$_{0/100*}$ and S~DVB@RT27/RT27$_{0/100}$ are gathered in Fig. 13b, giving values of 100.8, 103.9, 115.2, 92.04, 109.3 and 104.2 J g^{-1}, respectively. This latent heat values correspond with the contribution of the properly encapsulated paraffin, but also the energy from the paraffin that remains impregnating the surface of the capsules, since it can remain emulsified or simply adsorbed on the capsule surface. Analyzing the latent heats of the dried-washed capsules ($\Delta H_{S \sim DVB@RT27}$), it was found that they correspond with approximately a 70% of the non-washed ones, except for the materials S~DVB@RT27$_{70/30}$ and S~DVB@RT27$_{0/100*}$ with values of 78 and 75 %, respectively. These results confirm the presence of non-encapsulated paraffin in these slurries. This large amount of non-encapsulated paraffin of S~DVB@RT27$_{20/80*}$ and S~DVB@RT27$_{20/80}$ can explain the shifting of melting and crystallization temperature ranges towards higher temperatures. On the other hand, the developed slurries s-S~DVB@RT27$_{70/30}$, s-S~DVB@RT27$_{40/60}$, s-S~DVB@RT27$_{20/80*}$, s-S~DVB@RT27$_{20/80}$, s-S~DVB@RT27$_{0/100*}$ and s-S~DVB@RT27$_{0/100}$ exhibited large latent heats values 32.9, 32.8, 43.2, 25.9, 38.9 and 18.1 J g^{-1}, respectively. As expected, the two homogeneous slurries s-S~DVB@RT27$_{70/30}$ and s-S~DVB@RT27$_{40/60}$ presented similar latent heats because they have the same paraffin content in the whole liquid system and the higher latent heats were obtained for the slurries from the upper phases of the product, which can be explained for the lower density that presents the capsules with large paraffin content. On contrary, the slurries from the bottom phases of the products (s-S~DVB@RT27$_{20/80}$ and s-S~DVB@RT27$_{0/100}$) had the lower thermoregulating capacity.

Once the solid contents and the values of $\Delta H_{S \sim DVB@RT27/RT27}$ and $\Delta H_{S \sim DVB@RT27}$, were obtained for all the PCSs and considering the latent heat of pure

RT27 (ΔH_{PCM} = 168.4 J g^{-1}), the encapsulation parameters: EE, C_{PCM} and $\eta_{S\sim DVB@RT27}$, were determined. Attending to the data, C_{PCM} and EE are ranged within 40-50%, being the lowest EE obtained for the slurry s-S~DVB@RT27$_{20/80*}$, as result of its highest non-encapsulated paraffin amount. Finally, observing the encapsulation efficiency, the best reaction was performed producing the nano-slurry (s-S~DVB@RT27$_{40/60}$) with a particle yield ($\eta_{S\sim DVB@RT27}$) of 72.3 %. This particle yield was slightly higher than the value obtained for the sub-micron product s-S~DVB@RT27$_{70/30}$ (71.4 %) and much higher than those global particle efficiencies 65.9 and 66.8 %, for the sub-micron slurries from the phase change dispersions PCD$_{20/80}$ and PCD$_{0/100}$, respectively. Thus, the particle yield is favored when the reaction conditions were suitable for leading a single phase, and mainly when the final product has the properties of a nanomaterial.

Finally, the thermal reversibility of the optimal slurry product (s-S~DVB@RT27$_{40/60}$) and the PCD$_{40/60}$ were carried out by DSC analyses (Fig. 14). It can be observed that both thermal fluids work perfectly in a reversible way and also that the melting and crystallization of non-encapsulated paraffin tend towards higher temperatures and close to borders of the pure paraffin. Analyzing the long term-stability of s-S~DVB@RT27$_{40/60}$ after 100 heating/cooling cycles, negligible differences between DSC curves and nil losses in the latent heat storage capability were found; obtaining 32.7 J g^{-1} after 100 heating/cooling cycles, which is only 0.1 J g^{-1} less than the initial one. However, a supercooling of 15 °C is observed when using this type of PCM-based materials in liquid form, observing similar behavior for both the PCD and the NPCS, revealing significantly higher supercooling effect in liquid PCM products than for the pure paraffin, as reported in literature [59]. Anyway, the supercooling of PCD was slightly higher than for the s-S~DVB@RT27$_{40/60,}$ probably related to the fact that paraffin droplets can easily coalesce in emulsion, thus leading to larger supercooling [59],

whereas, in the case of the slurry, nanocapsules remain more stably dispersed in liquid media limiting aggregation. This increase of the PCM supercooling has been also observed previously when using nanometer-sized capsules in slurry form [60,61]. On contrary, the DSC results of the dried nano-capsules showed low supercooling (Fig. 13a). This can be explained by the fact that in bulk form one nucleation site can lead to the solidification of the whole volume by crystal growth, while, in an emulsion, every droplet has to be nucleated separately.

Additionally, making a comparison about the thermal advantage of this slurry respect to the water as cooling fluid can be estimated by integrating the DSC curve of the slurry within the solid-liquid transition temperature of RT27 (19-28 ºC). In this interval, water is only able to store 37.62 J/g of sensible heat provided by its C_p (4.18 J/(g·ºC) × 9 ºC), whereas the optimal slurry (s-S~DVB@RT27$_{40/60}$) is capable to store up to 56.3 J/g, combining both latent and sensible heat in the same temperature interval. So, for the operating temperature interval with interest for applying this slurry containing 17.8 wt% of RT27 as cooling thermal fluid, this slurry provides a thermal energy storage enhancement of a ~50% regarding the water employed as base fluid. Hence, the homogeneous NPCS (s-S~DVB@RT27$_{40/60}$) constituted by 28.1 wt% of nanocapsules with a $dn_{0.5}$ of 94.7 ± 15.0 nm and a latent heat of 74.6 J g^{-1}, presented the largest latent heat (32.8 J g^{-1}), Newtonian behavior, low viscosity (10.7 ± 0.3 mPa·s), large thermal reversibility and long-term colloidal stability ($|\zeta|$ =53.4 ± 1.8 mV fresh and $|\zeta|$ =55.8 ± 6.3 mV after two years); which are good properties to be considered as ideal thermal fluid for being applied in active thermal energy storage (TES) systems.

4. Conclusions

Thermoregulating slurries (PCSs) with latent heat values within 18.1-43.2 J g^{-1} were produced in a single process without waste generation by using mixtures of GA and SDS as surfactant agents, RT27 as PCM and S and DVB as monomers. The GA/SDS ratio affects the RT27 dispersion in water, generating PCDs with different breaking ratios and further PCSs with different properties. Homogeneous slurries were obtained for the case of using GA/SDS mass ratios of 70/30 and 40/60 (s-S~DVB@RT27$_{70/30}$ and s-S~DVB@RT27$_{40/60}$) whereas the GA/SDS mass ratios 20/80 or 0/100 led two phase products. The optimal GA/SDS ratio for the synthesis of a PCD that serves as PCS precursor has been found to be 40/60. The s-S~DVB@RT27$_{40/60}$ presented good colloidal stability ($|\zeta| = 64.1 \pm 3.2$ mV), the minimum breaking ratios fresh and after 15 days (1.7 and 2.1 vol%, respectively) and it is the only homogeneous one with nanometric droplet size (dn$_{0.5} = 94.7 \pm 15.0$ nm). Besides, it had a remarkable concentration (28.1 wt%) of NPCMs, exhibiting a large latent heat (32.8 J g^{-1}), long term thermal and colloidal stability (measured after two years of storing) and a Newtonian behavior with low viscosity (10.7 $\pm$ 0.3 mPa·s).

References

[1]   V. Siva Reddy, S.C. Kaushik, K.R. Ranjan, S.K. Tyagi, State-of-the-art of solar thermal power plants - A review, Renew. Sustain. Energy Rev. 27 (2013) 258–273. https://doi.org/10.1016/j.rser.2013.06.037.

[2]   M. Waterson, The characteristics of electricity storage, renewables and markets, Energy Policy. 104 (2017) 466–473. https://doi.org/10.1016/j.enpol.2017.01.025.

[3]   A. Inés Fernández, A. Solé, J. Giró-Paloma, M. Martínez, M. Hadjieva, A. Boudenne, M. Constantinescu, E. Maria Anghel, M. Malikova, I. Krupa, C. Peñalosa, A. Lázaro, H.O. Paksoy, K. Cellat, J. Vecstaudža, D. Bajare, B. Sumiga, B. Boh, T. Haussmann, S. Gschwander, R. Weber, P. Furmanski, M. Jaworski, L.F. Cabeza, Unconventional experimental technologies used for phase change materials (PCM) characterization: part 2 – morphological and structural characterization, physico-chemical stability and mechanical properties, Renew. Sustain. Energy Rev. 43 (2015) 1415–1426. https://doi.org/10.1016/J.RSER.2014.11.051.

[4]   E.M. Shchukina, M. Graham, Z. Zheng, D.G. Shchukin, Nanoencapsulation of phase change materials for advanced thermal energy storage systems, Chem. Soc. Rev. 47 (2018) 4156–4175. https://doi.org/10.1039/c8cs00099a.

[5]   M. Telkes, Thermal energy storage in salt hydrates, Sol. Energy Mater. 2 (1980) 381–393. https://doi.org/10.1016/0165-1633(80)90033-7.

[6]   A.M. Khudhair, M.M. Farid, A review on energy conservation in building applications with thermal storage by latent heat using phase change materials, Energy Convers. Manag. 45 (2004) 263–275. https://doi.org/10.1016/S0196-8904(03)00131-6.

[7]   L.F. Cabeza, A. Castell, C. Barreneche, A. De Gracia, A.I. Fernández, Materials used as PCM in thermal energy storage in buildings: A review, Renew. Sustain. Energy Rev. 15 (2011) 1675–1695. https://doi.org/10.1016/j.rser.2010.11.018.

[8]   H. Akeiber, P. Nejat, M.Z.A. Majid, M.A. Wahid, F. Jomehzadeh, I. Zeynali Famileh, J.K. Calautit, B.R. Hughes, S.A. Zaki, A review on phase change material (PCM) for sustainable passive cooling in building envelopes, Renew. Sustain. Energy Rev. 60 (2016) 1470–1497.

https://doi.org/10.1016/j.rser.2016.03.036.

[9]   A. Serrano, A.M. Borreguero, I. Garrido, J.F. Rodríguez, M. Carmona, Reducing heat loss through the building envelope by using polyurethane foams containing thermoregulating microcapsules, Appl. Therm. Eng. 103 (2016) 226–232. https://doi.org/10.1016/j.applthermaleng.2016.04.098.

[10] A.M. Borreguero, I. Garrido, J.L. Valverde, J.F. Rodríguez, M. Carmona, Development of smart gypsum composites by incorporating thermoregulating microcapsules, Energy Build. 76 (2014) 631–639. https://doi.org/10.1016/j.enbuild.2014.03.005.

[11] V.D. Cao, S. Pilehvar, C. Salas-Bringas, A.M. Szczotok, T.Q. Bui, M. Carmona, J.F. Rodriguez, A.-L. Kjøniksen, Thermal analysis of geopolymer concrete walls containing microencapsulated phase change materials for building applications, Sol. Energy. 178 (2019) 295–307. https://doi.org/10.1016/j.solener.2018.12.039.

[12] A.M. Borreguero, A. Serrano, I. Garrido, J.F. Rodríguez, M. Carmona, Polymeric-SiO_2-PCMs for improving the thermal properties of gypsum applied in energy efficient buildings, Energy Convers. Manag. 87 (2014) 138–144. https://doi.org/10.1016/j.enconman.2014.07.027.

[13] S.-J. Park, K.-S. Kim, S.-K. Hong, Preparation and thermal properties of polystyrene nanoparticles containing phase change materials as thermal storage medium, Polym. 29 (2005) 8–13.

[14] A. Jamekhorshid, S.M. Sadrameli, M. Farid, A review of microencapsulation methods of phase change materials (PCMs) as a thermal energy storage (TES) medium, Renew. Sustain. Energy Rev. 31 (2014) 531–542. https://doi.org/10.1016/J.RSER.2013.12.033.

[15] H. Liu, X. Wang, D. Wu, Innovative design of microencapsulated phase change materials for thermal energy storage and versatile applications: A review, Sustain. Energy Fuels. 3

(2019) 1091–1149. https://doi.org/10.1039/c9se00019d.

[16] J. Shi, X. Wu, R. Sun, B. Ban, J. Li, J. Chen, Nano-encapsulated phase change materials prepared by one-step interfacial polymerization for thermal energy storage, Mater. Chem. Phys. 231 (2019) 244–251. https://doi.org/10.1016/j.matchemphys.2019.04.032.

[17] S. Valizadeh, M. Ehsani, M. Torabí Angaji, Preparation, characterization and thermal properties of PCM nanocapsules with polystyrene/nano garaphen oxide shell for energy storage, Heat Mass Transf. Und Stoffuebertragung. 56 (2020) 575–586. https://doi.org/10.1007/s00231-019-02723-w.

[18] M. Delgado, A. Lázaro, J. Mazo, B. Zalba, Review on phase change material emulsions and microencapsulated phase change material slurries: Materials, heat transfer studies and applications, Renew. Sustain. Energy Rev. 16 (2012) 253–273. https://doi.org/10.1016/j.rser.2011.07.152.

[19] Z. Qiu, X. Ma, X. Zhao, P. Li, S. Ali, Experimental investigation of the energy performance of a novel Micro-encapsulated Phase Change Material (MPCM) slurry based PV/T system, Appl. Energy. 165 (2016) 260–271. https://doi.org/10.1016/j.apenergy.2015.11.053.

[20] L. Liu, Y. Jia, Y. Lin, G. Alva, G. Fang, Performance evaluation of a novel solar photovoltaic–thermal collector with dual channel using microencapsulated phase change slurry as cooling fluid, Energy Convers. Manag. 145 (2017) 30–40. https://doi.org/10.1016/j.enconman.2017.04.089.

[21] Z. Qiu, X. Ma, P. Li, X. Zhao, A. Wright, Micro-encapsulated phase change material (MPCM) slurries: Characterization and building applications, Renew. Sustain. Energy Rev. 77 (2017) 246–262. https://doi.org/10.1016/j.rser.2017.04.001.

[22] X. Huang, C. Zhu, Y. Lin, G. Fang, Thermal properties and applications of microencapsulated PCM for thermal energy storage: A review, Appl. Therm. Eng. 147

(2019) 841–855. https://doi.org/10.1016/j.applthermaleng.2018.11.007.

[23]   M. Jurkowska, I. Szczygieł, Review on properties of microencapsulated phase change materials slurries (mPCMS), Appl. Therm. Eng. 98 (2016) 365–373. https://doi.org/10.1016/J.APPLTHERMALENG.2015.12.051.

[24]   L. Fedele, L. Colla, S. Bobbo, S. Barison, F. Agresti, Experimental stability analysis of different water-based nanofluids, Nanoscale Res. Lett. 6 (2011) 1–8. https://doi.org/10.1186/1556-276X-6-300.

[25]   M.E. Meibodi, M. Vafaie-Sefti, A.M. Rashidi, A. Amrollahi, M. Tabasi, H.S. Kalal, The role of different parameters on the stability and thermal conductivity of carbon nanotube/water nanofluids, Int. Commun. Heat Mass Transf. 37 (2010) 319–323. https://doi.org/10.1016/j.icheatmasstransfer.2009.10.004.

[26]   W. Wu, H. Bostanci, L.C. Chow, Y. Hong, C.M. Wang, M. Su, J.P. Kizito, Heat transfer enhancement of PAO in microchannel heat exchanger using nano-encapsulated phase change indium particles, Int. J. Heat Mass Transf. 58 (2013) 348–355. https://doi.org/10.1016/j.ijheatmasstransfer.2012.11.032.

[27]   H. Gao, J. Wang, X. Chen, G. Wang, X. Huang, A. Li, W. Dong, Nanoconfinement effects on thermal properties of nanoporous shape-stabilized composite PCMs: A review, Nano Energy. 53 (2018) 769–797. https://doi.org/10.1016/j.nanoen.2018.09.007.

[28]   G. Sukhorukov, A. Fery, H. Möhwald, Intelligent micro- and nanocapsules, Prog. Polym. Sci. 30 (2005) 885–897. https://doi.org/10.1016/j.progpolymsci.2005.06.008.

[29]   J.P. Rao, K.E. Geckeler, Polymer nanoparticles: Preparation techniques and size-control parameters, Prog. Polym. Sci. 36 (2011) 887–913. https://doi.org/10.1016/j.progpolymsci.2011.01.001.

[30]   N. Anton, J.-P. Benoit, P. Saulnier, Design and production of nanoparticles formulated

from nano-emulsion templates-A review, J. Control. Release. 128 (2008) 185–199. https://doi.org/10.1016/j.jconrel.2008.02.007.

[31] C. Solans, P. Izquierdo, J. Nolla, N. Azemar, M.J. Garcia-Celma, Nano-emulsions, Curr. Opin. Colloid Interface Sci. 10 (2005) 102–110. https://doi.org/10.1016/j.cocis.2005.06.004.

[32] W. Wu, H. Bostanci, L.C. Chow, S.J. Ding, Y. Hong, M. Su, J.P. Kizito, L. Gschwender, C.E. Snyder, Jet impingement and spray cooling using slurry of nanoencapsulated phase change materials, Int. J. Heat Mass Transf. 54 (2011) 2715–2723. https://doi.org/10.1016/j.ijheatmasstransfer.2011.03.022.

[33] Y. Fang, H. Yu, W. Wan, X. Gao, Z. Zhang, Preparation and thermal performance of polystyrene/n-tetradecane composite nanoencapsulated cold energy storage phase change materials, Energy Convers. Manag. 76 (2013) 430–436. https://doi.org/10.1016/j.enconman.2013.07.060.

[34] W. Fu, X. Liang, H. Xie, S. Wang, X. Gao, Z. Zhang, Y. Fang, Thermophysical properties of n-tetradecane@polystyrene-silica composite nanoencapsulated phase change material slurry for cold energy storage, Energy Build. 136 (2017) 26–32. https://doi.org/10.1016/j.enbuild.2016.12.001.

[35] S. Barlak, O.N. Sara, A. Karaipekli, S. Yapıcı, Thermal Conductivity and Viscosity of Nanofluids Having Nanoencapsulated Phase Change Material, Nanoscale Microscale Thermophys. Eng. 20 (2016) 85–96. https://doi.org/10.1080/15567265.2016.1174321.

[36] A. Karaipekli, T. Erdoğan, S. Barlak, The stability and thermophysical properties of a thermal fluid containing surface-functionalized nanoencapsulated PCM, Thermochim. Acta. 682 (2019) 178406. https://doi.org/10.1016/j.tca.2019.178406.

[37] E.L. Kelley, W.J. Herzberg, J. V Sinka, Carbonaceous Oil Slurries Stabilized by Binary

Surfactant Mixtures, 1984. file:///C:/Users/Javier.Ramos/Documents/ITQUIMA (14.10.2019)/0. Bibliography/0. ITQUIMA/Slurries, PCM, Polymers/Kelley, E. L. US patent binary surfactant mixtures.pdf.

[38] E.P. Luther, F.F. Lange, D.S. Pearson, M. Colic, Development of Short-Range Repulsive Potentials by Short-Chain Surfactants in Aqueous Slurries, J. Am. Ceram. Soc. 82 (1999) 74–80. https://doi.org/10.1111/j.1151-2916.1994.tb07266.x.

[39] Y. Hong, S. Ding, W. Wu, J. Hu, A.A. Voevodin, L. Gschwender, E. Snyder, L. Chow, M. Su, Enhancing Heat Capacity of Colloidal Suspension Using Nanoscale Encapsulated Phase-Change Materials for Heat Transfer, ACS Appl. Mater. Interfaces. 2 (2010) 1685–1691. https://doi.org/10.1021/am100204b.

[40] H. Wang, W. Ma, J. Zhang, Z. Yang, D. Zong, Novel synthesis of silica coated palmitic acid nanocapsules for thermal energy storage, J. Energy Storage. 30 (2020) 101402. https://doi.org/10.1016/j.est.2020.101402.

[41] A.M. Borreguero, M. Carmona, M.L. Sanchez, J.L. Valverde, J.F. Rodriguez, Improvement of the thermal behaviour of gypsum blocks by the incorporation of microcapsules containing PCMS obtained by suspension polymerization with an optimal core/coating mass ratio, Appl. Therm. Eng. 30 (2010) 1164–1169. https://doi.org/10.1016/j.applthermaleng.2010.01.032.

[42] L. Sánchez-Silva, J. Tsavalas, D. Sundberg, P. Sánchez, J.F. Rodriguez, Synthesis and characterization of paraffin wax microcapsules with acrylic-based polymer shells, Ind. Eng. Chem. Res. 49 (2010) 12204–12211. https://doi.org/10.1021/ie101727b.

[43] Á. Alcázar, A.M. Borreguero, A. de Lucas, J.F. Rodríguez, M. Carmona, Microencapsulation of TOMAC by suspension polymerisation: Process optimisation, Chem. Eng. Res. Des. 117 (2017) 1–10. https://doi.org/10.1016/j.cherd.2016.10.005.

[44] A. Alcázar, M. Carmona, A.M. Borreguero, A. De Lucas, J.F. Rodríguez, Synthesis of microcapsules containing different extractant agents, J. Microencapsul. 32 (2015) 642–649. https://doi.org/10.3109/02652048.2015.1073385.

[45] Á. Alcázar, I. Garrido, E.M. García, A. De Lucas, M. Carmona, J.F. Rodriguez, New type of highly selective microcapsules for the removal of mercury from surface polluted waters, Sep. Purif. Technol. 154 (2015) 255–262. https://doi.org/10.1016/j.seppur.2015.09.043.

[46] I.A. Inc, The HLB System: A Time-saving Guide to Emulsifier Selection, ICI Americas, Incorporated, 1984. https://books.google.es/books?id=7KxuMwEACAAJ.

[47] M. Carmona Franco, J.F. Rodríguez Romero, A.M. Borreguero Simón, I. Garrido Sáenz, F.J. Ramos Mellado, D. López-Pedrajas, M. Jiménez-Vázquez, Procedimiento de obtención in situ de fluidos térmicos que contienen partículas termorreguladoras sub-micrónicas, ES2804063 A1, 2021. https://consultas2.oepm.es/InvenesWeb/detalle?referencia=P201930715.

[48] ISO, International Standard ISO 22412:2017 Particle size analysis - Dynamic light scattering (DLS), (2017).

[49] A. Lazaro, C. Peñalosa, A. Solé, G. Diarce, T. Haussmann, M. Fois, B. Zalba, S. Gshwander, L.F. Cabeza, Intercomparative tests on phase change materials characterisation with differential scanning calorimeter, Appl. Energy. 109 (2013) 415–420. https://doi.org/10.1016/j.apenergy.2012.11.045.

[50] B.J. Palla, D.O. Shah, Stabilization of high ionic strength slurries using the synergistic effects of a mixed surfactant system, J. Colloid Interface Sci. 223 (2000) 102–111. https://doi.org/10.1006/jcis.1999.6665.

[51] L.O. Orafidiya, F.A. Oladimeji, Determination of the required HLB values of some essential oils, Int. J. Pharm. 237 (2002) 241–249. https://doi.org/10.1016/S0378-5173(02)00051-

0.

[52]   D. Li, M.B. Müller, S. Gilje, R.B. Kaner, G.G. Wallace, Processable aqueous dispersions of graphene nanosheets, Nat. Nanotechnol. 3 (2008) 101–105. https://doi.org/10.1038/nnano.2007.451.

[53]   D. Hanaor, M. Michelazzi, C. Leonelli, C.C. Sorrell, The effects of carboxylic acids on the aqueous dispersion and electrophoretic deposition of ZrO_2, J. Eur. Ceram. Soc. 32 (2012) 235–244. https://doi.org/10.1016/j.jeurceramsoc.2011.08.015.

[54]   A. Dominguez, A. Fernandez, N. Gonzalez, E. Iglesias, L. Montenegro, Determination of Critical Micelle Concentration of Some Surfactants by Three Techniques, J. Chem. Educ. 74 (1997) 1227–1231. file:///C:/Users/Javier.Ramos/AppData/Local/Mendeley Ltd./Mendeley Desktop/Downloaded/Dominguez et al. - 1997 - Determination of Critical Micelle Concentration of Some Surfactants by Three Techniques.pdf.

[55]   A. Grein, B.C. Da Silva, C.F. Wendel, C.A. Tischer, M.R. Sierakowski, A.B.D. Moura, M. Iacomini, P.A.J. Gorin, F.F. Simas-Tosin, I.C. Riegel-Vidotti, Structural characterization and emulsifying properties of polysaccharides of Acacia mearnsii de Wild gum, Carbohydr. Polym. 92 (2013) 312–320. https://doi.org/10.1016/j.carbpol.2012.09.041.

[56]   J. Potočnik, Commission recommendation of 18 October 2011 on the definition of nanomaterial (2011/696/EU)., Off. J. Eur. Union. L275 (2011) 38–40. https://doi.org/10.2777/13162.

[57]   ISO, International Standard ISO/TS 80004-1. Nanotechnologies - Vocabulary - Part 1: Core terms, (2015).

[58]   A.M. Szczotok, I. Garrido, M. Carmona, A.-L. Kjøniksen, J.F. Rodriguez, Predicting microcapsules morphology and encapsulation efficiency by combining the spreading coefficient theory and polar surface energy component, Colloids Surfaces A

Physicochem. Eng. Asp. 554 (2018) 49–59. https://doi.org/10.1016/j.colsurfa.2018.06.022.

[59] S. Gschwander, S. Niedermaier, S. Gamisch, M. Kick, F. Klünder, T. Haussmann, Storage capacity in dependency of supercooling and cycle stability of different pcm emulsions, Appl. Sci. 11 (2021) 3612. https://doi.org/10.3390/app11083612.

[60] L. Huang, E. Günther, C. Doetsch, H. Mehling, Subcooling in PCM emulsions-Part 1: Experimental, Thermochim. Acta. 509 (2010) 93–99. https://doi.org/10.1016/j.tca.2010.06.006.

[61] E. Günther, L. Huang, H. Mehling, C. Dötsch, Subcooling in PCM emulsions - Part 2: Interpretation in terms of nucleation theory, Thermochim. Acta. 522 (2011) 199–204. https://doi.org/10.1016/j.tca.2011.04.027.

[62] M. Joseph, V. Sajith, An investigation on heat transfer performance of polystyrene encapsulated n-octadecane based nanofluid in square channel, Appl. Therm. Eng. 147 (2019) 756–769. https://doi.org/10.1016/j.applthermaleng.2018.10.120.

[63] Y. Fang, S. Kuang, X. Gao, Z. Zhang, Preparation of nanoencapsulated phase change material as latent functionally thermal fluid, J. Phys. D. Appl. Phys. 42 (2009) 05407. https://doi.org/10.1088/0022-3727/42/3/035407.

[64] M. Tafavogh, A. Zahedi, Improving the performance of home heating system with the help of optimally produced heat storage nanocapsules, Renew. Energy. 181 (2022) 1276–1293. https://doi.org/10.1016/j.renene.2021.07.015.

[65] M.R. Hashemi Jirandeh, M. Mohammadiun, H. Mohammadiun, M.H. Dubaie, M. Sadi, Intelligent modeling of rheological and thermophysical properties of nanoencapsulated pcm slurry, Heat Transf. 49 (2020) 2080–2102. https://doi.org/10.1002/htj.21709.

[66] M. Jiménez-Vázquez, F.J. Ramos, I. Garrido, D. López-Pedrajas, J.F. Rodríguez, M.

Carmona, Production of thermoregulating slurries constituted by nanocapsules from melamine-formaldehyde containing n-octadecane, J. Energy Storage. 51 (2022) 104465. https://doi.org/10.1016/j.est.2022.104465.

Figures caption

Fig. 1. PCD and PCS synthesis scheme.

Fig. 2. Effect of sonication time and input energy per PCD volume on droplet size ($dv_{0.5}$, $dn_{0.5}$) and $|\zeta|$, using 17.8 wt% of PCM content stabilized with a GA/SDS mass ratio (40/60). Error bars were expressed as a point (mean) with whiskers representing the confidence interval.

Fig. 3. a) PCDs breaking ratio depending on the GA/SDS mass ratios both fresh and after 15 days. b) Picture of the PCDs prepared from GA/SDS mass ratios of 100/0 and 40/60 after 15 days of settling.

Fig. 4. Influence of GA/SDS mass ratio on PCDs, fresh and after 15 days a) $|\zeta|$ and b) $dv_{0.5}$ and $dn_{0.5}$. Error bars were expressed as a point (mean) with whiskers representing the confidence interval.

Fig. 5. Surface tension of the PCDs and the mixture water cosurfactant, for GA/SDS mass ratios of 100/0, 70/30, 40/60, 20/80 and 0/100. Error bars were expressed as a point (mean) with whiskers representing the confidence interval.

Fig. 6. a) Phase separation of the different synthesized products after 2 days. b) Photograph of the products from GA/SDS mass ratios of 100/0 and 40/60.

Fig. 7. PSD of the capsules contained in the synthesized slurries a) in number and b) in volume.

Fig. 8. a) $dv_{0.5}$ and b) $dn_{0.5}$ from the PCDs, compared with those from the synthesized PCSs. Error bars were expressed as a point (mean) with whiskers representing the confidence interval.

Fig. 9. HRSEM images of the PCM capsules contained in synthesized PCSs.

Fig. 10. Rheological analysis of different slurries displaying a) shear stress and b) viscosity as a function of shear rate (1 - 250 - 1 s^{-1}) at 20 ºC, with a pre-shearing at 100 s^{-1}.

Fig. 11. Colloidal stability ($|\zeta|$) of PCDs and PCSs, freshly manufactured and aged two years. * means de the upper phase of the PCSs with two phases. Error bars were expressed as a point (mean) with whiskers representing the confidence interval.

Fig. 12. a) TGA of the PCSs manufactured in this work. b) First derivate of TGA curve (DTGA) for those PCSs.

Fig. 13. a) DSC of synthesized S~DVB@RT27 and pure RT27, b) Histogram graph summarizing the latent heat for the S~DVB@RT27/RT27 and s-S~DVB@RT27 and c) EE (Eq. 3), C_{PCM} (Eq. 2) and $\eta_{S\sim DVB@RT27}$ (Eq. 4) plot for all synthesized PCSs.

Fig. 14. Thermal heating/cooling cycling (- 10 to 40 ºC) for the NPCS s-S~DVB@RT27$_{40/60}$ and the PCD$_{40/60}$ by DSC.

Figure 1.
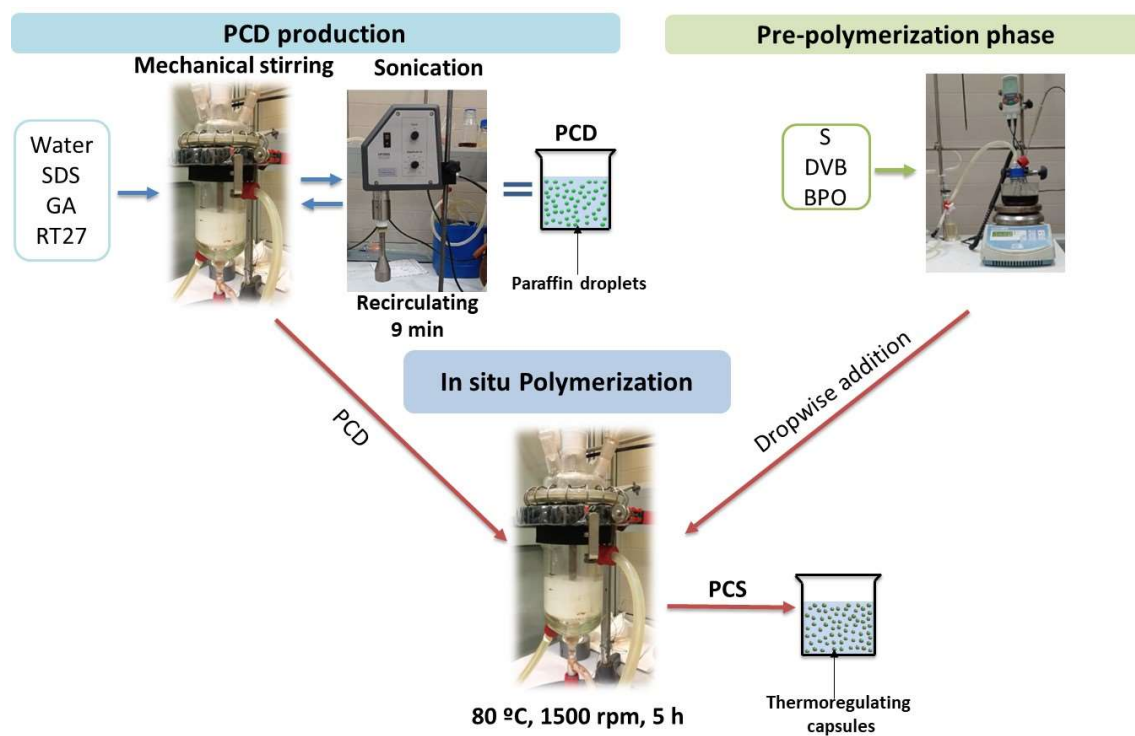
Figure 2.
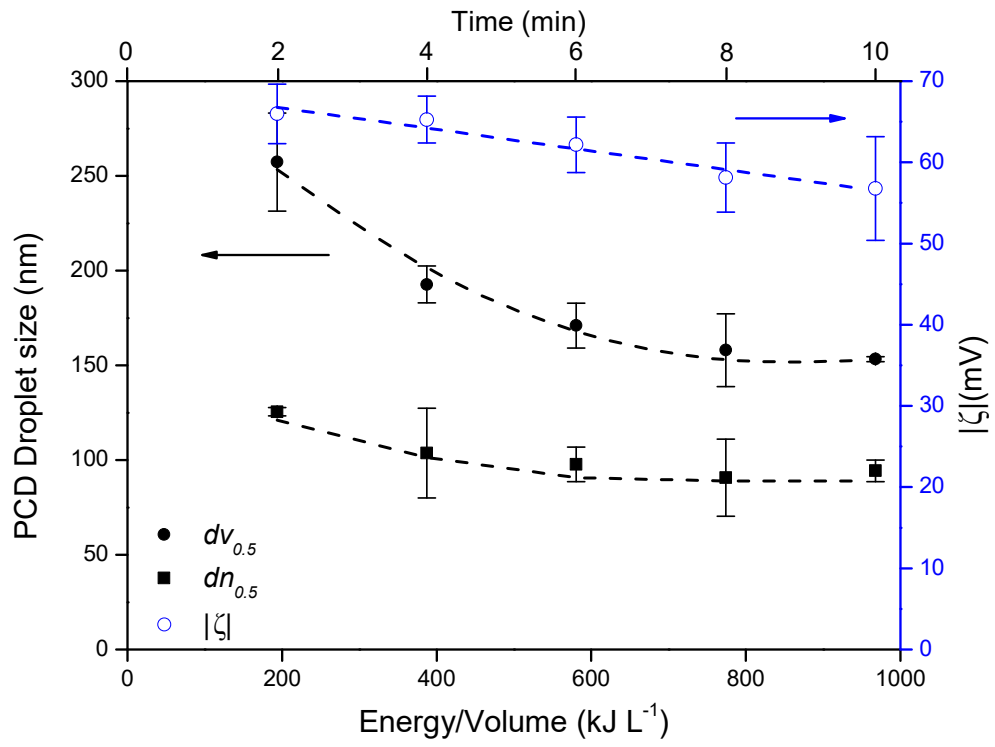
Figure 3.
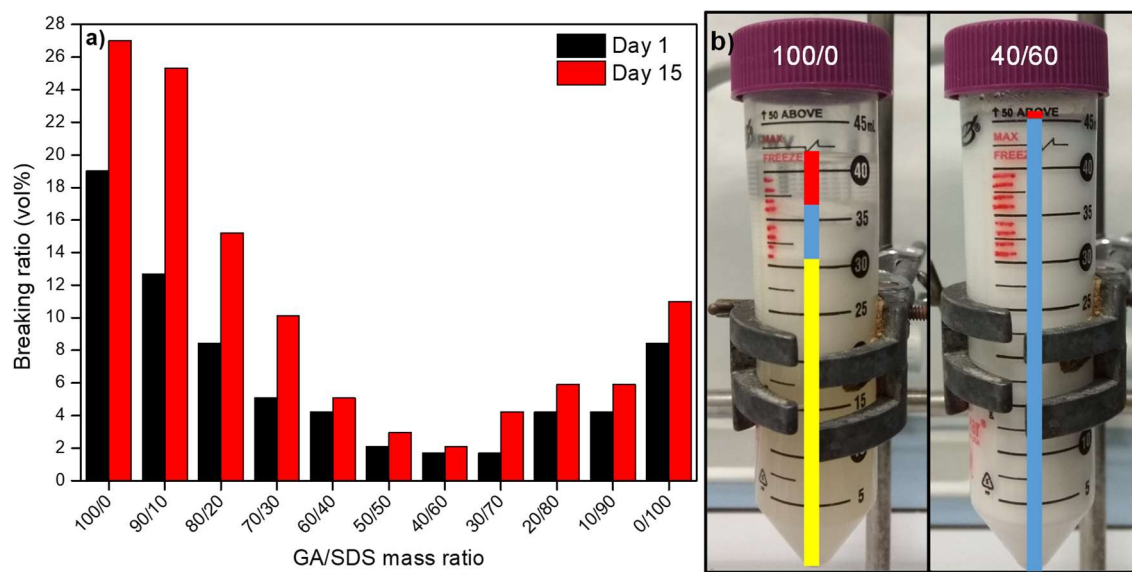
Figure 4.
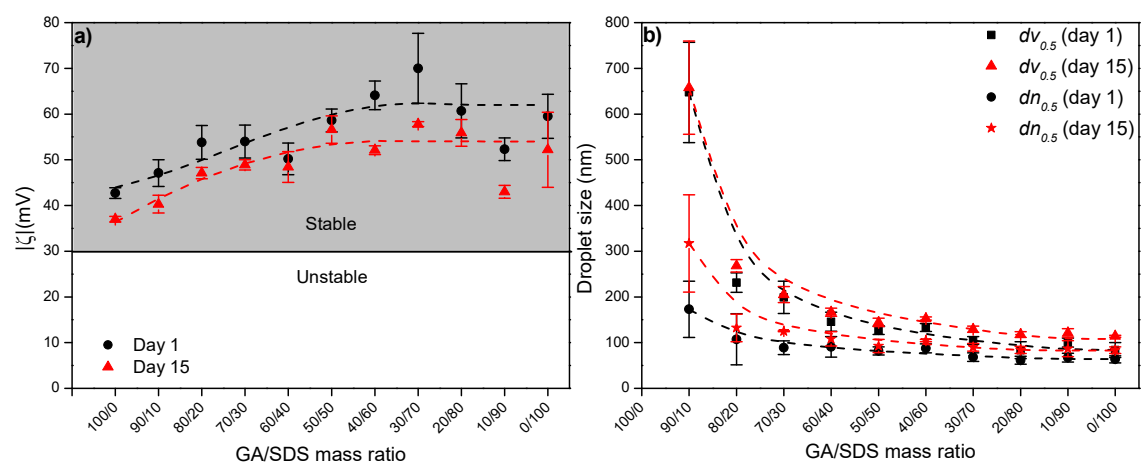
Figure 5.
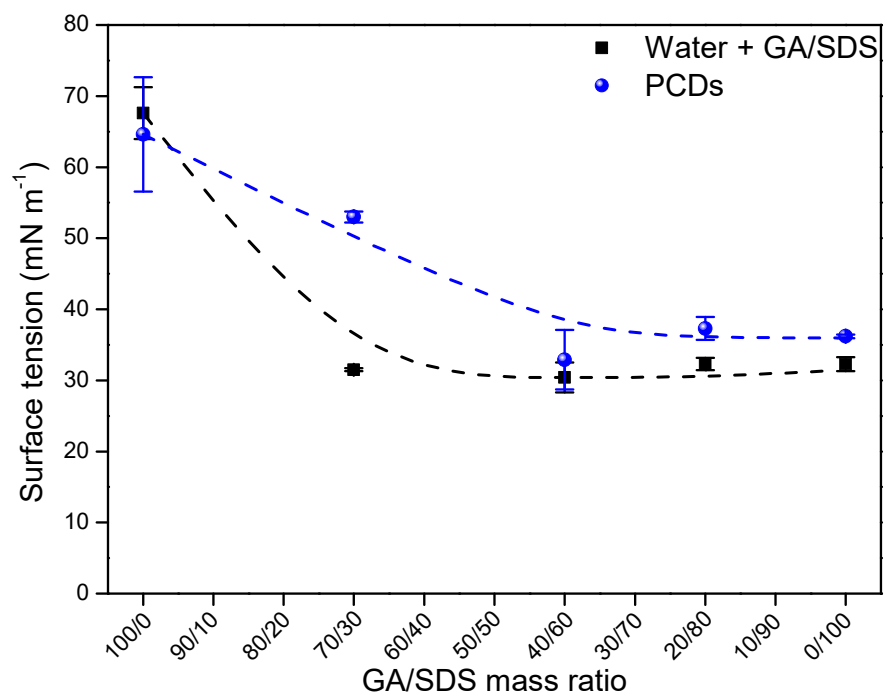
Figure 6.
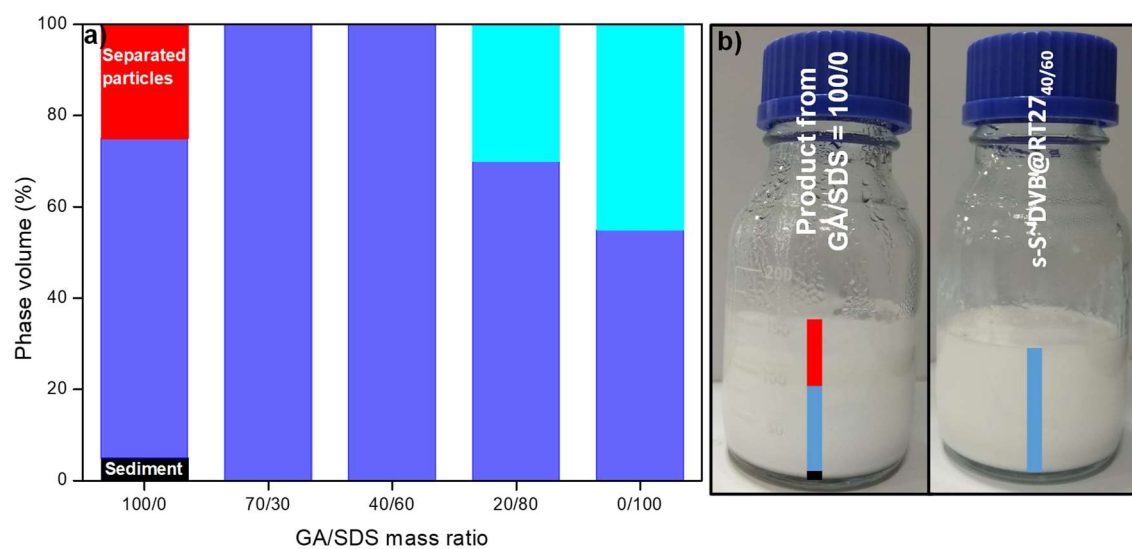
Figure 7.
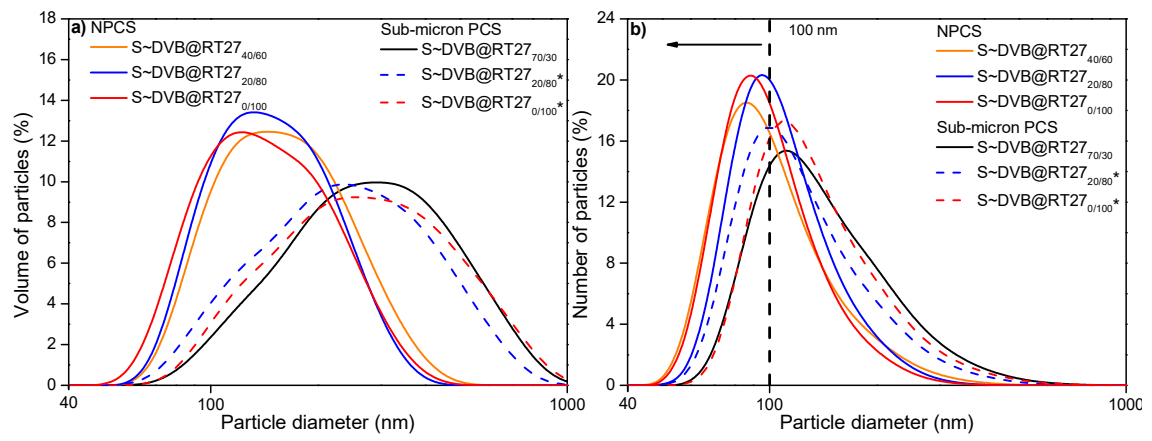
Figure 8.
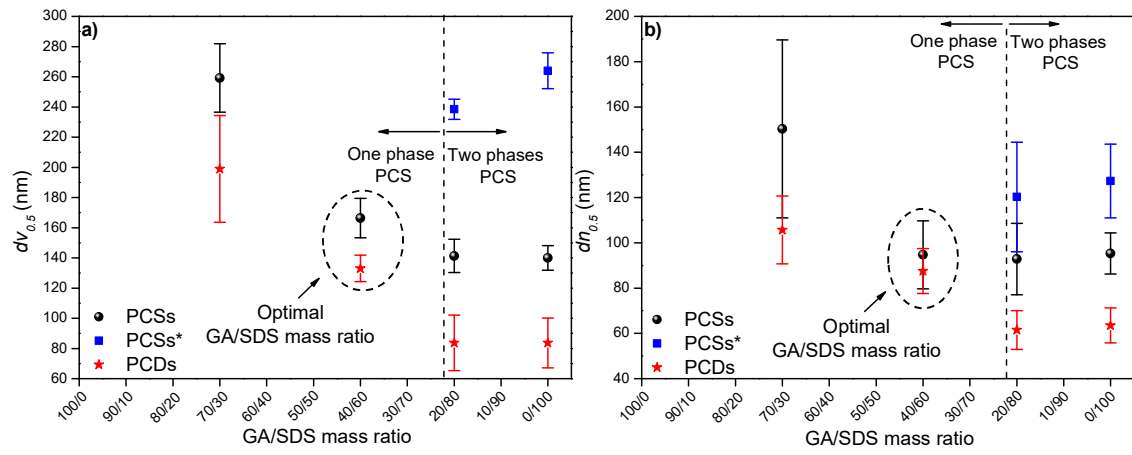
Figure 9.
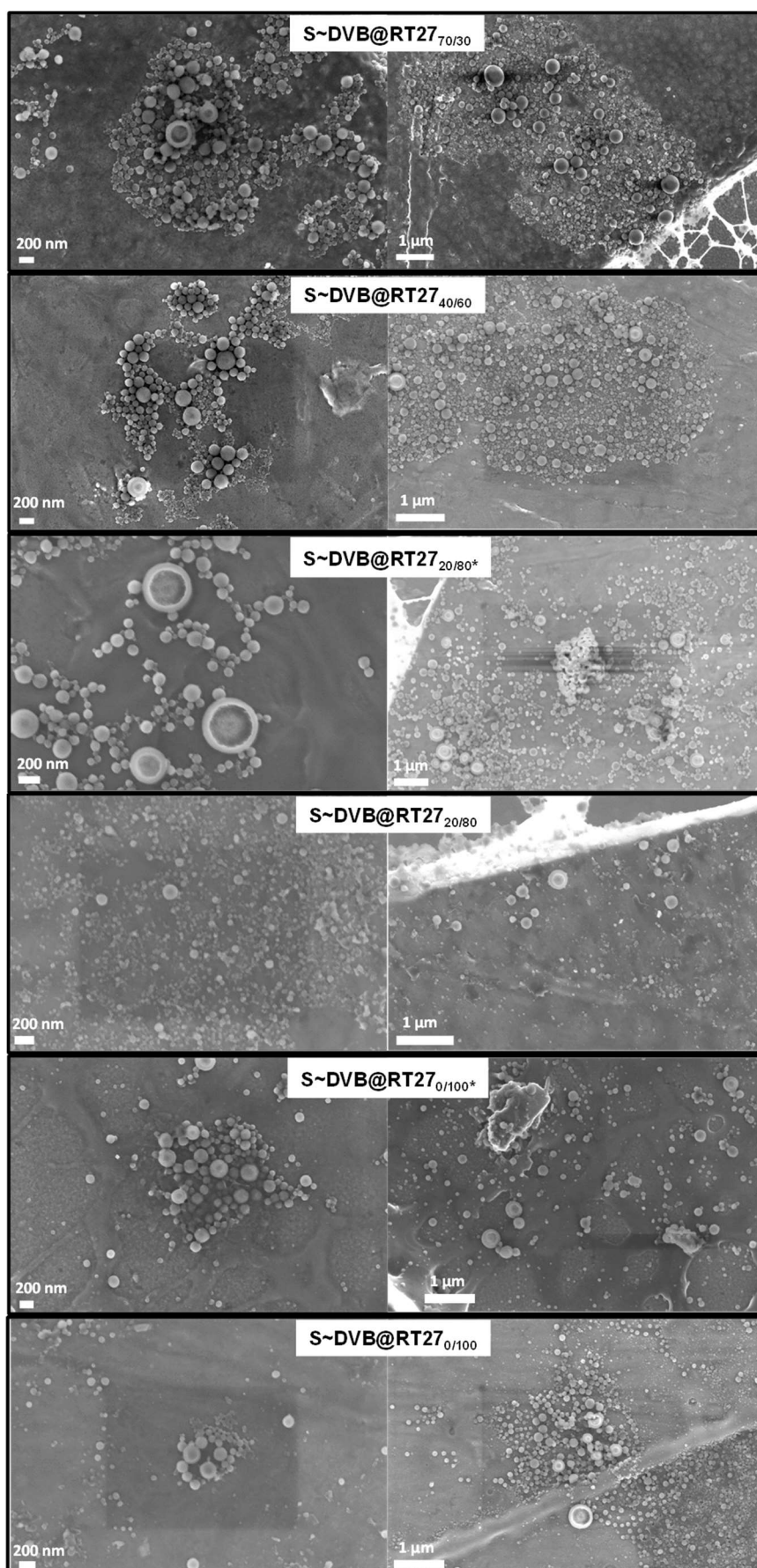
Figure 10.
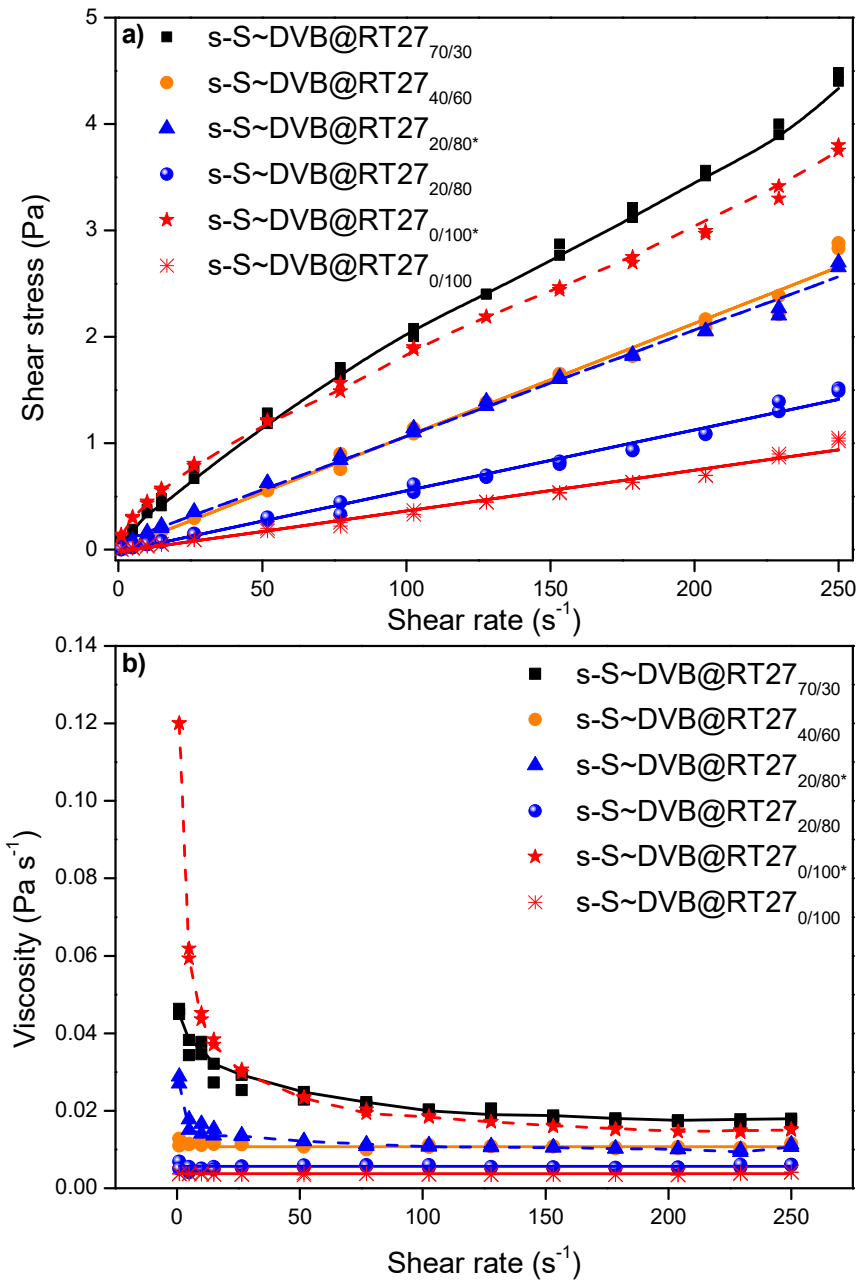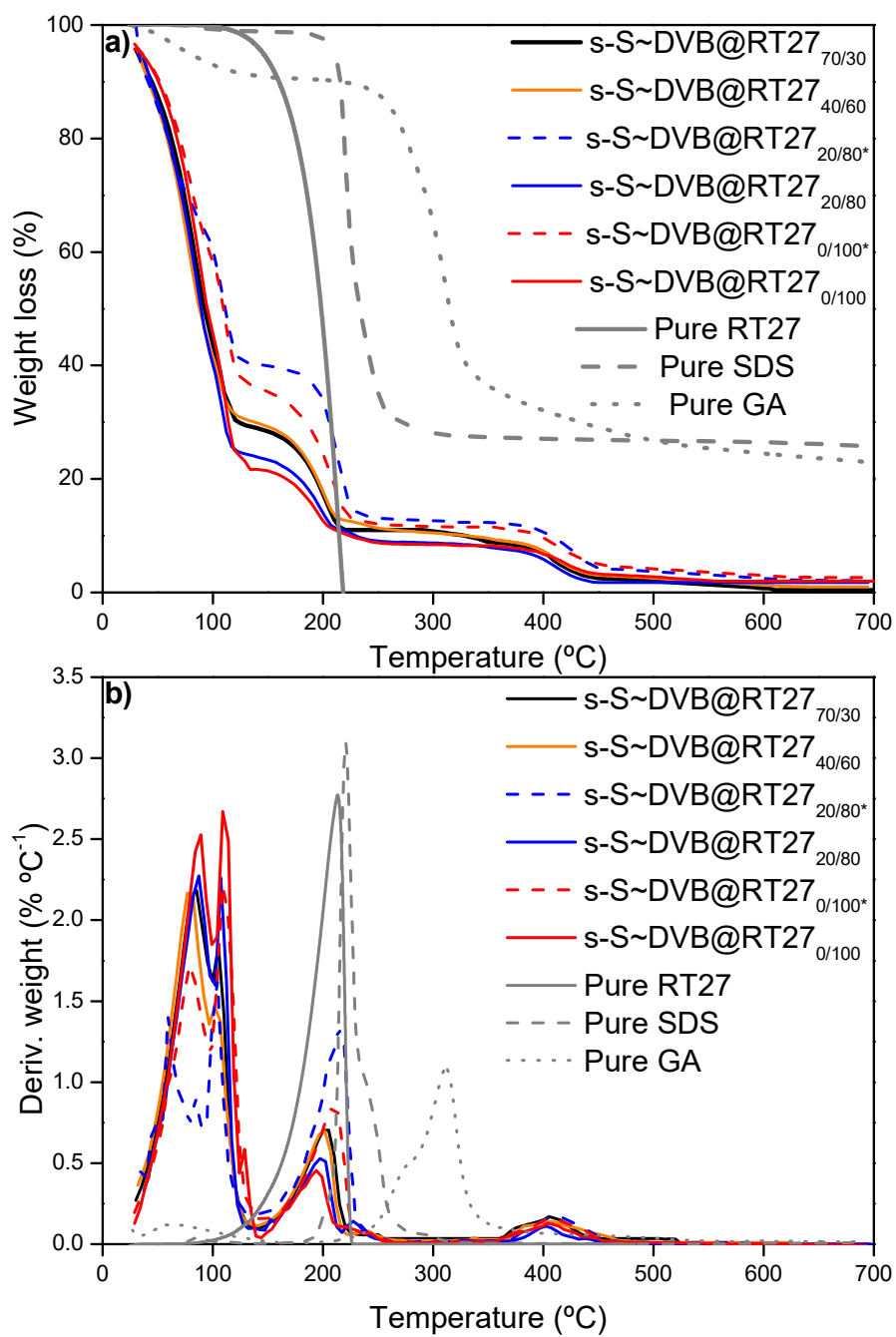
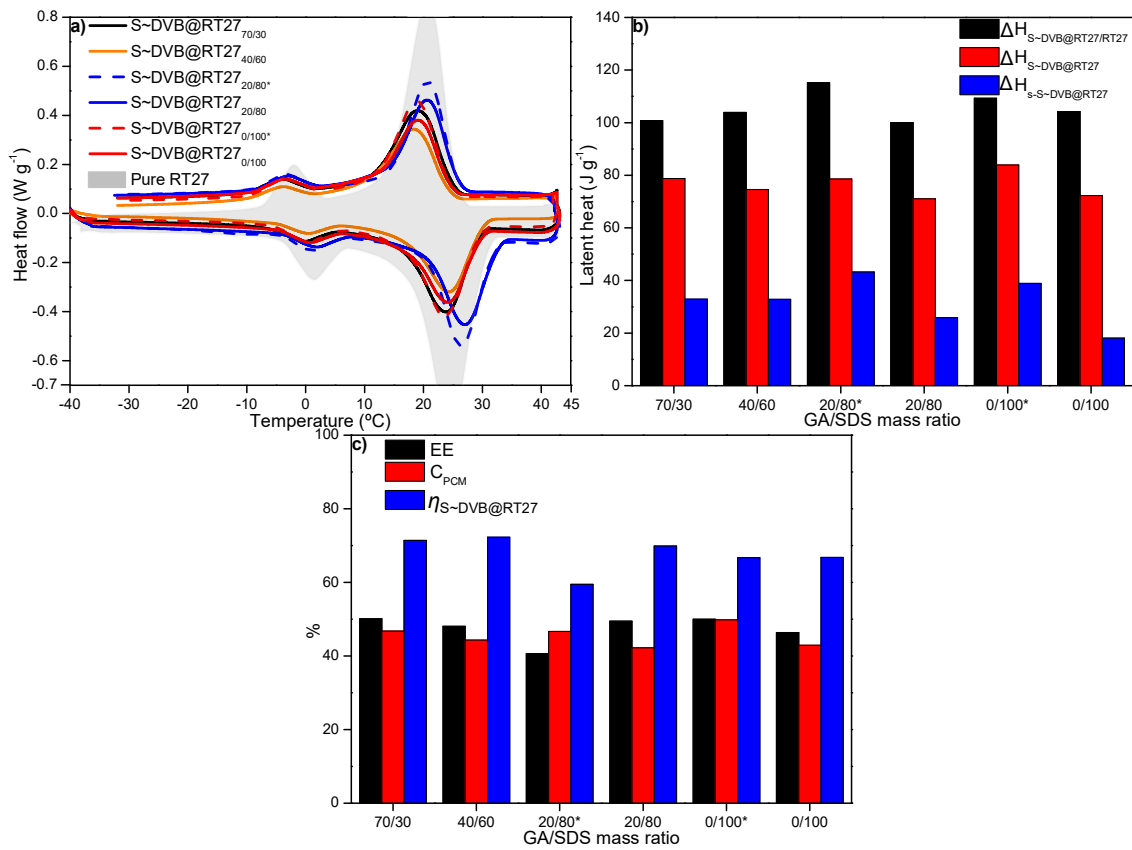**Figure 11.**
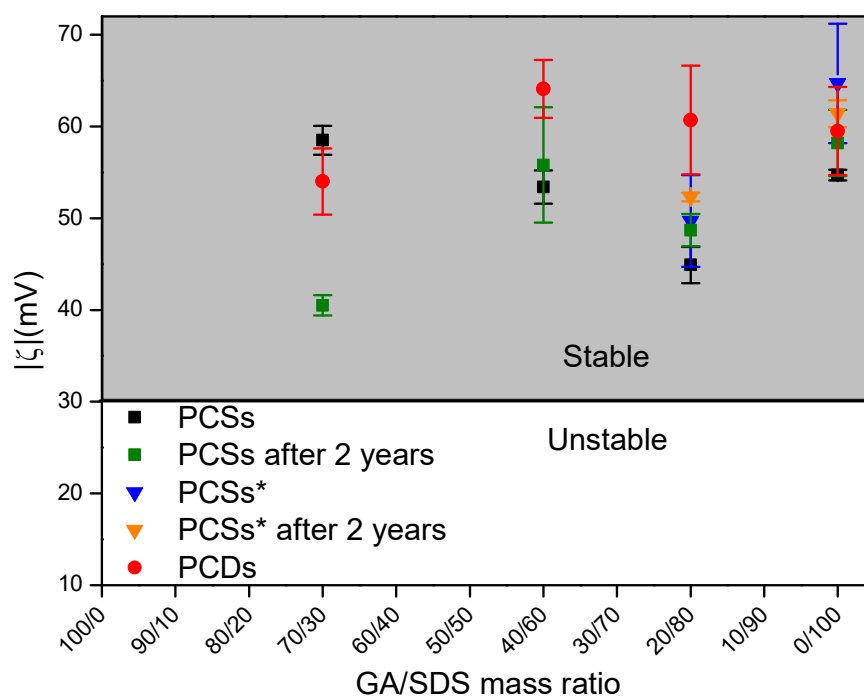
Figure 12.
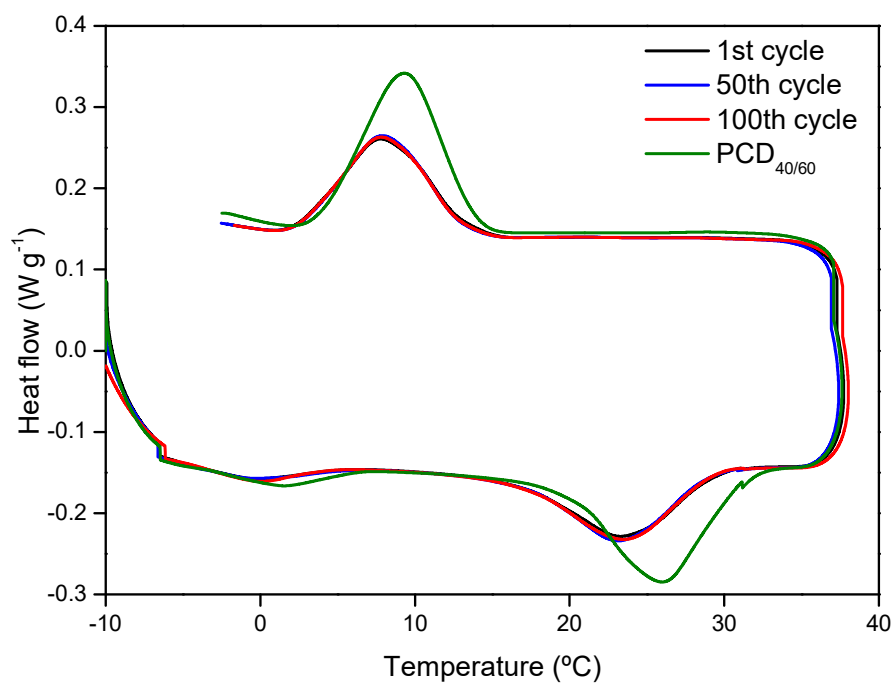
Figure 13.

Figure 14.

Table 1. Solids content, capsule diameter (dc), $|\zeta|$, $\Delta H_{Capsules}$, C_{PCM}, μ and ΔH_L of the synthesized SPCSs and NPCSs found in literature.

Shell@core	Solids content	dc (nm)	$\|\zeta\|$ (mV)	$\Delta H_{Capsules}$ (J g⁻¹)	C_{PCM} (%)	μ (mPa s)	ΔH_L (J g⁻¹)
P(S~EA)@Tet [33]	3.8[c]	132	-	98.71	44.7	2.7	3.7[a]
	7.5[c]					7.4	7.4[a]
	15[c]					14.8	14.8[a]
PS@C18 [62]	0.25-10[c]	209	53-70	133.7	53.7	1.2-1.3[b]	0.3-13.4[a]
P(S~MMA)-SiO₂@Tet [34]	5[c]	151.3	-	83.4	37.8	2.1	4.2
PS@C18 [32]	15[d]	100	-	107.1	48.6	1.4	15.6
	28[d]					2.7	31.2
	40[d]					8.6	44.6
P(S~MAA)@C19 [36]	2[c]	212	56.8	89.12	54.0	1.19	1.8[a]
P(S~AA)@C18 [39]	-	200	-	110.1	47.4	1.0[f]	-
P(S~AA~BA~MMA)@C18 [63]	20.6[c]	124		124.4	53.5	3.6[f]	11.6
PU@C19 [35]	3.4[d]	103	-	92.8	43.8	1.5	-
P(MMA~EHA)@C18 [64]	20.0[c]	600	-	65.5	27.0	-	13.1[a]
PS@AP25 [65]	5.0[c]	SPCM	-	132.2	77.6	~10[g]	6.6[a]
	15.0[c]					~70[g]	19.8[a]
	25.0[c]					~1000[g]	33.0[a]
P(M~F)@C18 [66]	14.4[c]	63.7	50	125.9	50	4.0[f]	23.0

[a] PCSs property theoretically calculated from $\Delta H_{Capsules}$ and the solids content

[b] They only calculated the viscosity until the 1.5 vol%

[c] wt%

[d] vol%

[f] measured at 25 ºC

[g] measured at 5 ºC

Abbreviations. dc: capsule diameter, EA: Ethyl acrylate, Tet: n-Tetradecane, C18: n-Octadecane, MMA: Methyl methacrylate, MAA: Methacrylic acid, C19: n-Nonadecane, AA: Acrylate acid, BA: Butyl acrylate, PU: Polyurethane and EHA: Ethyl Hexyl acrylate, M: Melamine, F: Formaldehyde.

Table 2. List of the materials used for PCDs and PCSs production.

REAGENT	PURITY	SUPPLIER
Styrene (S)	99 %	Sigma-Aldrich Chemical Co.
Divinylbenzene (DVB)	80 %	Sigma-Aldrich Chemical Co.
NaOH pellets	97 %	Panreac Co.
Sodium dodecyl sulfate (SDS)	90 %	Panreac Co.
Gum arabic (GA)	Reactive grade	Sigma-Aldrich Chemical Co.
Benzoyl peroxide (BPO)*	Pharma grade	Panreac Co.
Rubitherm®RT27 (RT27)		Rubitherm GmbH
Water	Milli-Q	
Ethanol	96 %	Guinama

* Humidified with ∼25 wt% of H_2O

Table 3. Recipe for the PCSs synthesis with different GA/SDS mass ratios.

Products	Content (wt%)						
	Water	GA	SDS	RT27	S	DVB	BPO
s-S~DVB@RT27$_{100/0}$		3.5	-				
s-S~DVB@RT27$_{70/30}$		2.5	1.0				
s-S~DVB@RT27$_{40/60}$	67.7	1.4	2.1	17.8	4.45	4.45	2.0
s-S~DVB@RT27$_{20/80}$		0.7	2.8				
s-S~DVB@RT27$_{0/100}$		-	3.5				